Evaluation of Two Automated Remote Sensing-Based Surface Energy Balance Models for Estimating Daily Evapotranspiration

Lynn Duijndam

Delft University of Technology

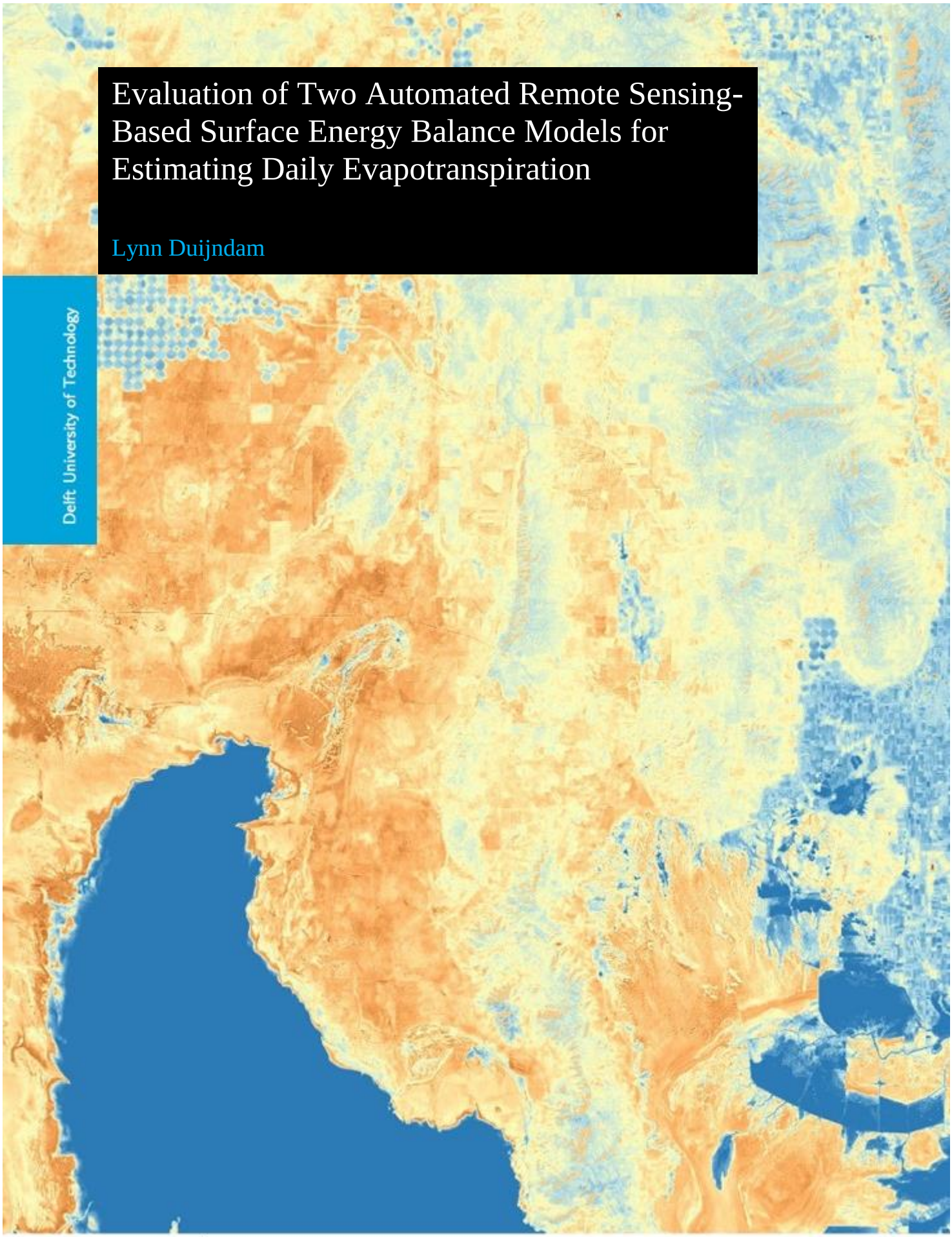

TU Delft Delft University of Technology

Challenge the future

Evaluation of Two Automated Remote Sensing-Based Surface Energy Balance Models for Estimating Daily Evapotranspiration

By

Lynn M. Duijndam

in partial fulfilment of the requirements for the degree of

Master of Science
in Civil Engineering

at the Delft University of Technology,
to be defended publicly on Friday October 28, 2016 at 2:30 PM.

Supervisor:	Prof. dr. W.G.M. Bastiaanssen,	TU Delft
Thesis committee:	Dr. ir. A.M.J Coenders-Gerrits,	TU Delft
	Dr. S.M. Alfieri,	TU Delft
	Dr. J.D. van Opstal,	UNESCO-IHE

TU Delft

Abstract

Remote sensing based surface energy balance models are often used to produce actual evapotranspiration (ET) estimates over large spatial scales, which provide vital information of water consumption for many water resources applications. In the past these models have required trained users for a model calibration process, which needed to be completed during every model run. This requirement limited the number of people capable of acquiring the data and the speed at which ET estimates could be generated. Two of these remote sensing based surface energy balance models have recently been automated: the automated Surface Energy Balance Algorithm for Land (SEBAL3.0) and Earth Engine Evapotranspiration Flux (EEFlux). Automation of these models increases the number of potential users and increases the speed at which estimations can be produced.

In this study SEBAL3.0 and EEFlux have been used to produce daily ET estimates for locations around the world with different climates and land covers. These results were compared with ground measurements from flux tower systems to evaluate the performance of the models. In addition to comparing daily ET estimates to flux tower measurements, SEBAL3.0 estimates for other surface energy balance components were compared to flux tower measurements. Eighteen flux tower sites were split into two sets. Set 1 was used for the initial model runs and for a calibration of constants used to calculate the hot and cold anchor pixel surface temperatures from the group of hot and cold pixels identified by SEBAL3.0. Set 2 was used for additional runs for EEFlux and for validation of the calibrated constants developed using Set 1.

Set 1 SEBAL3.0 results showed systematic underestimations of daily ET caused by systematic overestimations of the sensible heat flux. Set 1 EEFlux results showed significantly different performance levels between the sites in the Netherlands and the sites in the United States. The Netherlands' sites had many unreasonable over and underestimates for daily ET. Set 1 SEBAL3.0 daily ET estimates had a RMSE of 2.48 mm/d and EEFlux daily ET estimates had a RMSE of 6.24 mm/d. A calibration performed using select sites and days from Set 1 sites showed a variation between optimal constant values on a spatial and temporal scale. New constants were selected based on the constant combinations with the majority of optimum combinations.

Although no changes were made to EEFlux between Set 1 and Set 2 runs, Set 2 daily ET results had an improved RMSE of 4.46 mm/d. Set 2 EEFlux results did not have the same unreasonable estimations as Set 1, however, several sites estimated negative daily ET rates for many days. Set 2 SEBAL3.0 results had a slightly improved RMSE of 4.16 mm/d with the calibrated constants. SEBAL3.0 inaccurately selected cold pixels for two sites in very dry semi-arid regions due to a lack of water bodies. Although there was still a large amount of scatter, sensible heat flux results improved from the calibration and were no longer systematically underestimated. SEBAL3.0 24 hr averaged net radiation for both sets showed a reasonable fit with the measurement data.

The cumulative values of all daily ET estimates for each site were calculated for SEBAL3.0, EEFlux and flux tower measurements. SEBAL3.0 cumulative estimates had percent errors ranging from 12% to 132% and 4 out of 6 sites had cumulative errors under 20%. EEFlux cumulative estimates had percent errors ranging from 4% and 176% and only 1 out of 6 sites had a cumulative error under 20%.

Acknowledgments

First I would like to thank my daily supervisor Wim Bastiaanssen for his guidance during my thesis. I would also like to thank him for connecting me with the contacts who provided me with flux tower data for sites around the world. I would like to thank Jonna van Opstal for her daily support, especially for her help with interpreting flux tower data from different sources and her help with any problems I encountered while running models. I would also like to thank the other committee members, Miriam Coenders-Gerrits and Silvia Alfieri, for their comments and suggestions on my report.

Finally I would like to thank all the personal contacts who allowed me to use their flux tower data.

Contents

List of Figures

List of Tables

List of Abbreviations

AUS	Australia
BRA	Brazil
DEM	Digital Elevation Map
DOY	Day of Year (1-365)
EC	Eddy Covariance
EEFlux	Earth Engine Evaporation Flux
METRIC	Mapping EvapoTranspiration at high Resolution with Internalized Calibration
NASA	National Aeronautics and Space Administration
NLD	the Netherlands
NOAA	National Oceanic and Atmospheric Administration
SEBAL	Surface Energy Algorithm for Land
TUN	Tunisia
USA	United States of America
USGS	United States Geological Survey
ZAF	South Africa

1 Introduction

Actual evapotranspiration (ET) data is important for many water resources planning and management applications due to the large influence of ET on the hydrological cycle. ET is referred to as the sum of the loss of water to the atmosphere from both evaporation from the land surface and transpiration from vegetation. ET data is often used to determine agricultural water consumption and optimize irrigation practices. Other applications of the data include climate modeling, drought monitoring, and development of water budgets. ET is spatially variable because it is influenced by the following spatially varying factors: land covers, vegetation types, soil characteristics and precipitation patterns [1]. Field measurements of actual evaporation can be obtained from eddy covariance systems, lysimeters, scintillometers, water balance studies, and Bowen ratio systems. However, these methods can only measure point values or ET averaged over a limited area. Data from these field measurement methods do not give information on the spatial distribution over larger areas needed for many water resources applications.

ET measurements at larger spatial scales can be estimated with satellite remote sensing data. Remote sensing ET models can be divided into global and field scale models. Global models provide global coverage for ET estimations at coarser resolutions than field scale models. Examples of global models include the MODIS Global Evapotranspiration Project (MOD16) with 1km resolution, the Surface Energy Balance System (SEBS) model with 1km resolution, and the Global Land Evaporation Amsterdam Model (GLEAM) with a 0.25 degree resolution. Field scale models, such as the Surface Energy Balance Algorithm for Land (SEBAL) developed by Bastiaanssen [2] and the Mapping Evapotranspiration at high Resolutions with Internalized Calibration (METRIC) model [3], can estimate daily ET values at higher resolutions for a specific area of interest smaller than a few hundred kilometers. Several satellite data products can be used as model inputs for these field scale models, however, in this study, Landsat images are used resulting in spatial resolutions of 30 m.

SEBAL and METRIC estimate daily ET values using remotely sensed satellite data from visible, near infrared, and longwave (thermal) bands, and the energy balance. Using satellite data combined with meteorological data, it is possible to calculate ET values from the latent heat flux which is solved for as the residual of the land surface energy balance using Eq. (1) [4].

$$\lambda E = R_n - G - H \qquad (1)$$

where λE is the latent heat flux associated with evaporation (W/m^2), R_n is the net radiation (W/m^2), G is the soil heat flux (W/m^2) and H is the sensible heat flux (W/m^2).

Typically remote sensing based surface energy balance algorithms require expert users for calibration. SEBAL and METRIC require trained users for the selection of pixels for calibration, which is a subjective procedure and can affect model results [5] [6]. However, both of these models have recently developed automated versions. This study used SEBAL3.0, the automated SEBAL model, and Earth Engine Evapotranspiration Flux (EEFlux), the automated METRIC model. Both SEBAL3.0 and EEFlux have been developed to have automated operation and calibration. These field scale models are the first automated remote sensing based surface energy balance models using Landsat images to estimate daily ET rates a 30 m resolution.

1.1 Problem Statement

SEBAL and METRIC have both been typically used to model for agricultural areas. They provide farmers or irrigation managers with important information about water consumption in their fields. Since Landsat satellite data is used, the models are able to produce results at 30 m spatial resolutions which allows for analysis of water use for each individual field. This information is also important for water regulation and water rights in areas with limited water supply. Both SEBAL and METRIC require a trained user to calibrate the models for each Landsat scene. A trained user is required because an accurate selection of the hot and cold pixels is important for calibrating each image for the sensible heat flux. Even with trained users, the hot and cold pixel selection calibration by different users will result in a range of results [7]. With the automation of the newly developed SEBAL3.0 and EEFlux, the models can be used by a much broader group of users who do not need to have specific training. This group includes irrigation or water resources managers and consultants, as well as scientists. A goal of EEFlux is to give farmers access to water maps for their fields in near real-time from their smartphones [8]. Automation also saves time that was previously required for manual pixel selection and results can be generated faster than with the non-automated versions. Results can be produced within several seconds or minutes as soon as satellite data is available, allowing for results that are near real-time.

The automation of the models uses the computer to perform a procedure that was previously completed manually. The models are able to calculate daily ET rates for anywhere on the planet where Landsat data is available. This means the automated procedure has to perform for different climates and landscapes. To determine if the automation affected the performance of the models it was necessary to validate the models. It is important for the models to have accurate results for many applications such as irrigation management. Validation of the models was required to ensure the models produce accurate and trustworthy estimates for applications such as water rights allocation and irrigation management.

1.2 Research Objectives

The objective of this study was to test the performance of these recently developed automated models (SEBAL3.0 and EEFlux) against flux tower measurement data from areas with different climates and land covers. Flux tower sites were selected in areas with different climates, land covers, and irrigation types to assess if the models performed better under certain conditions. The selected climates included: arid, semi-arid, Mediterranean, temperate, humid continental and tropical. Land cover types of the selected sites included some natural landscapes and a variety of crops with some irrigated and some rain-fed.

One of the main goals was to evaluate the accuracy of SEBAL3.0 and METRIC in estimated daily ET rates using flux tower measurement as the ground truth. In addition to analysis on daily evapotranspiration results, this study evaluated the performance of other energy balance components from SEBAL3.0 including: sensible heat flux, net radiation, soil heat flux and evaporative fractions. The evaporative fraction is used to calculate daily ET from instantaneous values and is calculated as the ratio of latent heat flux to available energy (R_n-G). The results from energy balance component comparisons with measured flux tower data were used to make adjustments to SEBAL3.0 with the aim of improving modeled estimations.

This report aims to investigate the following research question:

Can automated remote sensing-based surface energy balance models SEBAL3.0 and EEFlux provide estimates of daily evapotranspiration similar to ground measured flux tower values?

1.3 Report Structure

In Chapter 2 a description of the automated models and flux tower systems used in this study will be provided. The methods of closure for the eddy covariance flux tower data and the procedure for the calibration of a component of the SEBAL3.0 model will also be discussed. Chapter 3 gives an overview of all the study sites and a description of each site. In Chapter 4 comparisons of EEFlux and SEBAL3.0 daily ET rates with flux tower measurements will be shown and analysed. Comparisons of other SEBAL3.0 energy flux components with flux tower measurements will also be shown and discussed. Overall performance of the two automated models will be discussed in Chapter 5 and conclusions will be given in Chapter 6.

2 Materials and Methods

2.1 SEBAL3.0

SEBAL3.0 is the recently developed automated version of SEBAL which is programmed in Python. The model has automated calibration, however, it requires users to input some meteorological data and has several general constants that can be adjusted by the user. The model calculates net radiation, soil heat flux, and sensible heat flux, then uses the surface balance, Eq. (1), to calculate latent heat flux. SEBAL uses the evaporative fraction to upscale instantaneous ET values to daily values. The following equations in this section are from the SEBAL3.0 code [9].

Inputs

SEBAL3.0 calculations require meteorological data inputs of air temperature, humidity, wind speed and solar radiation at the time of satellite over pass (instantaneous values) and the 24 hr averaged values. For most study sites these inputs were obtained from local meteorological stations. For sites where local meteorological data could not be acquired, Global Land Assimilation System Version 2 (GLDAS-2) data was used for model inputs. GLDAS uses land surface models to generate flux and land surface state parameters. In this study data was acquired from the NOAH 3.3 land surface model with a 3 hour temporal resolution and a spatial resolution of 0.25°. Instantaneous data values were taken as the 3 hourly value that included the time of overpass. Twenty-four hour averaged data was calculated by averaging the eight 3 hourly values on the day of interest. GLDAS data is acquired from NASA's Earth Science Division [10].

Landsat images for inputs were acquired from Landsat 5, 7 and 8 depending on the date of availability of flux tower data per site. Landsat 5 was operated by NASA and NOAA. It was launched in March 1984 and collected data until January 2013. Landsat 5's Thematic Mapper (TM) images consisted of seven spectral bands including one thermal band. Landsat 7 was launched in April 1999 and is still collecting data today. In 2003 the Landsat 7 scan line corrector failed, resulting in data gaps in all scenes after this failure. Landsat 7's Enhanced Thematic Mapper Plus (ETM+) images consist of eight spectral bands including one thermal band. Landsat 8 was launched in February 2013 and is presently still collecting data. Landsat 8's Operational Land Imager (OLI) and Thermal Infrared Sensor (TIRS) images consist of 11 bands including 2 thermal bands. Landsat 7 and 8 are both operated by NASA and USGS [11]. Landsat image bands have 30 m spatial resolutions with the exception of the thermal and panchromatic bands. The thermal bands are resampled to 30 m resolutions. Shuttle Radar Topography Mission (SRTM) 1 Arc-Second Global data was used for the SEBAL3.0 DEM input [12].

Net Radiation

To compute the net radiation, the following surface radiation balance equation is used:

$$R_n = (1-\alpha)R_{s\downarrow} + R_{L\downarrow} - R_{L\uparrow} - (1-\varepsilon_0)R_{L\downarrow} \quad (2)$$

where α is surface albedo, $R_{s\downarrow}$ is incoming shortwave radiation (W/m^2), $R_{L\downarrow}$ is incoming longwave radiation (W/m^2), $R_{L\uparrow}$ is outgoing longwave radiation (W/m^2), and ε_0 is surface emissivity. Surface albedo is the ratio of reflected radiation to the incident shortwave radiation. It is calculated using the satellite measured narrow band spectral radiances. Incoming shortwave radiation is one of the required

input parameters for the model. The incoming longwave radiation is calculated using the Stefan-Boltzmann equation with atmospheric emissivity and the meteorological input of air temperature. The outgoing longwave radiation is calculated using the Stefan-Boltzmann equation with surface emissivity and surface temperature.

Soil Heat Flux

Soil heat flux is the rate of heat energy transferred from the earth's surface to the subsurface. It is calculated using Eq. (3) and is a function of the net radiation, surface temperature, albedo and normalized difference vegetation index (NDVI). NDVI accounts for the amount and condition of green vegetation and is calculated using the reflectivity from the visible (red) band and a near infrared band (Band 4 for Landsat 5 and 7, and Band 5 for Landsat 8).

$$G = R_n\,(T_s\,(0.0038 + 0.0074\,\alpha)(1 - 0.978\,NDVI^4)) \qquad (3)$$

Sensible Heat Flux

Sensible heat flux is the rate of heat energy transferred from the earth's surface to the atmosphere by conduction and convection [13]. The sensible heat flux is a function of the temperature gradient, surface roughness and wind speed. SEBAL3.0 estimates the sensible heat flux using the following heat transfer equation:

$$H = \frac{\rho\, c_\rho\, \mathrm{d}T}{r_{ah}} \qquad (4)$$

where ρ is the air density (kg/m^3), c_ρ is the specific heat of air at constant pressure (J/kg K), dT is the vertical near surface temperature difference (K) and r_{ah} is the aerodynamic resistance to heat transport (s/m). An iterative procedure is needed to solve for H and r_{ah}. The aerodynamic resistance to heat transport is needed to solve for H and H is needed to make a correction to r_{ah} to account for the effects of buoyancy of heated, light air at the surface [1]. A flow chart of the entire iterative procedure can be found in Appendix A. This section will further discuss the use of the near surface temperature difference (dT) in estimating the H.

The near surface temperature difference represents a temperature difference between two heights z_1 and z_2. This temperature difference is used because satellites measure radiometric temperature which can differ from aerodynamic temperature by several degrees [3]. It is assumed that a linear relationship exists between dT and T_s. This relationship is represented in Eq. (5).

$$\mathrm{d}T = a\,T_s + b \qquad (5)$$

where a and b are calibration coefficients. A hot and cold anchor pixel are selected to determine the relationship between dT and T_s. A plot of the relationship between dT and T_s with hot and cold pixels is shown in Figure 1. The cold pixel is selected from a wet location which is assumed to have no sensible heat flux (H=0). The hot pixel is selected as a dry, bare location which is assumed to have no latent heat flux. The sensible heat flux at this location can be calculated as H=R_n-G. Using the inverse of Eq. (4) the dT for the cold and hot pixel can be calculated as:

$$\mathrm{d}T = H\,\frac{r_{ah}}{\rho * c_\rho} \qquad (6)$$

With the linear relationship in Eq. (5) it is possible to calculate a dT for all surface temperatures on a Landsat scene and then use Eq. (4) to solve for the sensible heat flux.

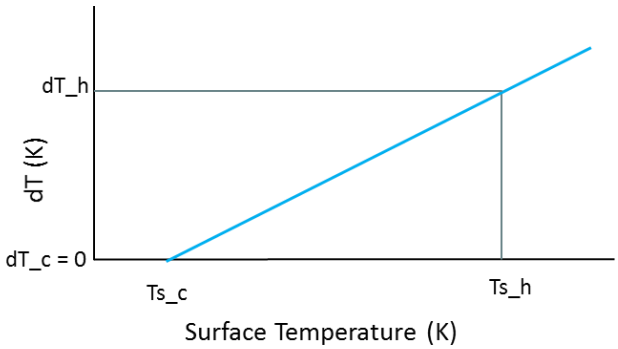

Figure 1: Linear relationship between dT *and surface temperature (T_s) derived from known values from hot and cold anchor pixels. "c" indicates cold and "h" indicates hot.*

Since SEBAL3.0 is automated, the pixel selection procedure is not performed by the user. The model selects a group of pixels to be the hot pixels and a group of pixels to be the cold pixels based on NDVI values, surface temperatures, and the water mask. Hot pixels are selected as the locations where NDVI values are greater than or equal to a set NDVI hot low limit and where NDVI values are smaller than or equal to a set NDVI hot high limit. For this study NDVI_hot_low was set to 0.03 and NDVI_hot_high was set to 0.20. Pixels are excluded if they are identified as water by a water mask, if they are identified as a cloud by a cloud mask or if they are identified as a shadow by the shadow mask. They are also excluded if the surface temperature of the pixel is below 273 K. All pixels that meet these criteria are selected as part of the hot pixel group. Cold pixels are selected as areas that are identified as water by a water mask. Satellite reflectance data is used to calculate a water mask for each Landsat scene. Cold pixels within the water mask are excluded if they are identified as a cloud or shadow by the cloud mask and shadow mask. They are also excluded if the surface temperature of the pixel is below 273 K. All pixels that meet these criteria are selected as part of the cold pixel mask. If no water is identified by the water mask then cold pixels are identified based on cold vegetation pixels. These cold vegetation pixels are selected using NDVI values and a NDVI threshold calculated using the maximum and standard deviation for NDVI values on each select day. No Landsat scenes used in this study selected cold pixels based on cold vegetation. The water mask identified water areas for each scene. The cloud and shadow mask are used to identify and remove pixels in areas that have cloud or shadow cover. These pixels are removed because they often have lower surface temperatures which can affect the selection of cold pixels. A majority of Landsat scenes selected in this study were cloud free.

The surface temperature selected as T_{s_hot} and T_{s_cold} is calculated from the mean, standard deviation and minimum temperature of each group of pixels, and a constant for the hot and cold calculation. Eqs. (7) and (8) show these calculations. The rest of the SEBAL3.0 procedure for calculating sensible heat flux is the same as the SEBAL procedure described earlier in this section.

$$T_{s\_hot} = T_{s\_hot\_mean} + (hot\_constant)\, T_{s\_hot\_std} \quad (7)$$

$$T_{s\_cold} = T_{s\_cold\_min} + (cold\_constant)\, T_{s\_cold\_std} \quad (8)$$

Pixel Selection Constant Adjustment

The first step of this study was to run both SEBAL3.0 and EEFlux for locations from one set of flux tower sites. An overview and description of all flux tower sites is in Chapter 3. The estimates of daily ET from both models were compared to the flux tower measurements to evaluate model performance. The performance of SEBAL3.0 in estimating all flux terms was also evaluated by a comparison of

model results to flux tower measurements. Based on these results, adjustments were made to the sensible heat flux calculation in an attempt to improve performance.

To adjust the sensible heat flux, calculated from Eq. (4), adjustments were made to the selected surface temperatures for both the hot and cold pixels. These changes affected the dT which, depending on the changes, raised or lowered the calculated sensible heat flux. If higher surface temperatures were selected to represent the T_s values for the hot and cold pixels, the adjusted T_s/dT relationship would shift. This shift would result in surface temperatures with lower dT values than from the old relationship. Figure 2 shows the dT/T_s relationship with the effects of the hot and cold pixels T_s adjustment.

In SEBAL3.0 the original calculation for T_{s_hot} and T_{s_cold} are given in Eqs. (7) and (8). T_{s_hot} was calculated using the mean surface temperature of the group of hot pixels plus 2 times the standard deviation of surface temperature of the group of hot pixels. To adjust the surface temperature of the hot pixel, the constants +2, +3 and +4 were tested. T_{s_cold} was calculated using the minimum surface temperature from the group of cold pixels plus 0.5 times the standard deviation of surface temperature of the group of cold pixels. This equation was adjusted to use the mean instead of the minimum to prevent the effects that could result from an outlier being used as the minimum surface temperature. For the cold pixel, instead of 0.5 times the standard deviation, the constants -2, -1, 0, +1, and +2 were tested. All fifteen combinations of hot and cold pixel surface temperature selection constants were tested for two overpass days at three sites. A final pixel selection was chosen from these results and a second set of flux tower data sets was used to validate the adjustments.

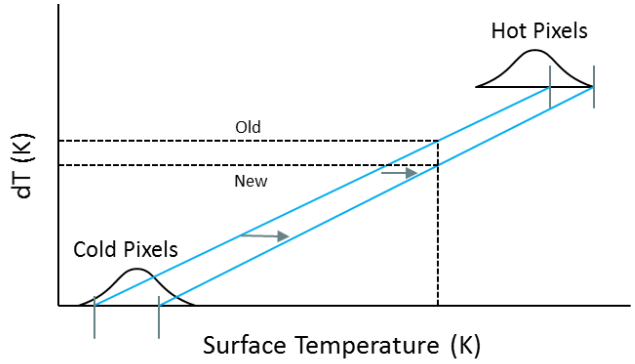

Figure 2: Adjustment of T_s for hot and cold pixel selection in SEBAL3.0.

Evaporative Fraction

The previously calculated net radiation, soil heat flux and sensible heat flux all represent instantaneous values at time of satellite overpass. The instantaneous latent heat flux can be calculated as the residual from these values. To upscale instantaneous ET to 24 hr ET the evaporative fraction (EF) is used. EF is calculated with Eq. (9) and is defined as the ratio of latent heat flux to available energy (R_n-G) [4].

$$EF_{inst} = \frac{\lambda E}{\lambda E + H} = \frac{R_n - G - H}{R_n - G} \qquad (9)$$

Instantaneous EF is converted to 24 hr averaged EF using an advection factor (AF), Eq. (10), to account for any effects of regional advection. This advection factor is used in Eq. (11) to calculate 24 hr ET.

$$AF = 1 + 0.985\left(\exp\left((e_{sat\_24} - e_{act\_24})\ 0.08\right) - 1.0\right) EF_{inst} \qquad (10)$$

$$ET_{24} = EF_{inst}\,(AF)\,\frac{R_{n_{24}}}{\lambda * \rho_w}\,86400000 \quad (11)$$

where e_{sat_24} is 24 hr averaged saturated vapor pressure (kPa) and e_{act_24} is 24 hr averaged actual vapor pressure (kPa), λ is the latent heat of vaporization (J/kg) and ρ_w is the density of water (kg/m^3).

2.2 EEFlux

Earth Engine Evapotranspiration Flux is a fully automated evapotranspiration mapping tool that operates on the Google Earth Engine [14]. It was developed as a joint effort between the University of Nebraska-Lincoln, the Desert Research Institute, the University of Idaho, and Google. Similar to SEBAL3.0, EEFlux estimates ET at a 30 m spatial resolution using Landsat images and the surface energy balance.

The user interface of the model makes it simple to use. Users select their desired location and time frame for analysis. The model displays all of the available Landsat 5, 7, or 8 images for the specified time and location, and the percentage of cloud cover for each image. The user can select the desired Landsat image as the input and run the model. Various outputs including albedo, NDVI, DEM, land cover, surface temperature, and reference ET can be viewed in the user interface. Outputs of the reference ET fraction (ET_rF) and actual daily evapotranspiration can be viewed and downloaded.

EEFlux uses a variety of data sources for weather data, soil data, land use data, and digital elevation maps [15]. For the continental United States, gridded weather is acquired from the North American Land Assimilation System (NLDAS) [16], GridMET [17], and Real Time Mesoscale Analysis (RTMA) for recent dates where NLDAS data is not available [18]. Gridded weather data for areas outside the continental United States is acquired from the Climate Forecast System Version 2 (CSFV2) [19]. Soil data is used in EEFlux to produce time series of evaporation from bare soil. The NRCS State Soil Geographic (STATSGO) Data Base is used for soil data from the continental United States [20]. The FAO soils data base and Global Soil database [21] are used for all other areas. The National Land Cover Database (NLCD) is used for land use data for the United States [22]. Land cover maps for areas outside the United States are acquired from the European Space Agency's Climate Change Initiative (CCI) global land cover data product [23].

EEFlux is based on METRIC, which originated from earlier versions of SEBAL. As METRIC has developed it has deviated from SEBAL. Some of the main differences include the method used to compute daily ET from instantaneous values, and the cold and hot pixel sensible heat calculation.

METRIC uses the reference ET fraction (ET_rF) to compute daily ET values from instantaneous values. ET_rF, calculated by Eq. (12), is the ratio of the instantaneous ET to the reference ET (ET_r) [1]. ET_r is the ET rate for 0.5 m tall alfalfa at the time of the image. It is calculated using the standardized ASCE Penman-Monteith equation using weather data [24].

$$ET_rF = \frac{ET_{inst}}{ET_r} \quad (12)$$

METRIC assumes the instantaneous ET_rF is the same as the 24 hr averaged ET_rF. This reference ET fraction is multiplied by the 24 hr ET_r to calculate the daily ET in Eq. (13) [1]. ET_{r_24} is the sum of the

hourly reference ET rates on the day of interest. METRIC requires hourly weather data for the entire day to calculate the hourly reference ET rates.

$$ET_{24} = ET_rF \text{ x } ET_{r\_24} \quad (13)$$

METRIC also calculates the sensible heat flux from the cold anchor pixel using a different method than SEBAL. METRIC does not select the cold pixel from a body of water, instead a pixel is selected from a wet irrigated field. An assumption is made that wet irrigated fields, with leaf area indices (LAI) greater than 4, have ET rates about 5% larger than the ET_r rate [1]. This assumption is made because the wet soil beneath fully covered fields can cause the ET rate to be higher than ET_r. Using this assumption, METRIC calculates H_{cold} for a cold pixel in an irrigated field using Eq. (14) [1].

$$H_{cold} = R_n - G - 1.05\, ET_r \quad (14)$$

In METRIC during the non-growing season, a ratio of ET_{cold} to ET_r is developed as a function of NDVI. This relationship is developed by the user based on the Landsat image or on local data.

Automated Pixel Selection

An automated calibration algorithm for METRIC was previously designed for an automated pixel selection [7]. This procedure iteratively selected hot and cold pixels and checked the distribution of ET_rF values resulting from the selected pixels until ET_rF distributions were similar to that of trained users [7]. There is currently no model description or metadata available for EEFlux data, so the exact automation procedure is unknown. EEFlux likely uses the same automated pixel selection procedure as the automated METRIC which is described in this section. The remainder of this subsection describes the automated METRIC procedure developed by Morton *et al.* [7] and Allen *et al.* [25].

The automated pixel selection in METRIC begins by outlining an area of interest. This area of interest consists of agricultural land and is identified using a land cover map. A filtering procedure is used to exclude pixels on the edge of fields which may include non-agricultural areas outside the field. This area of interest is cut down to a group of potential hot and cold pixels using NDVI values and surface temperatures. Identification of the cold pixel group begins by selecting pixels with NDVI's in the top 5% of the area of interest. From these top 5% NDVI pixels, the coldest 20% surface temperature pixels are selected. The averaged surface temperature is calculated from this selection of cold pixels (coldest 20% of the highest 5% NDVI pixels). The final cold pixel group are pixels with a surface temperature within ± 0.2 K of the calculated average cold surface temperature and an albedo that is within ± 0.2 of an albedo threshold calculated as a function of the sun angle above the horizon [26]. Identification of the hot pixel group begins by selecting pixels with NDVI's in the lowest 10% from the agricultural area of interest. From this lowest 10% NDVI pixel population, the hottest 20% surface temperature pixels are selected. The averaged surface temperature is calculated from this selection of hot pixels (hottest 20% of the lowest 10% NDVI pixels). The final hot pixel group are pixels with a surface temperature within ± 0.2 K of the calculated average hot surface temperature.

When hot and cold pixels are selected and METRIC is run using these pixels, a distribution of the resulting ET_rF values can be made. The hot pixel is generally placed at a pixel with an ET_rF of about 1.05 and the cold pixel is generally placed at a pixel with an ET_rF of about 0.1. For each Landsat image the percentage of pixels with ET_rF values above the threshold of 1.05 and below the threshold of 0.1 can be found by looking at the ET_rF distribution. This percentage above or below the threshold is referred to as the tail size percentage. The ET_rF distributions from multiple users, seasons, Landsat

scenes and years were used to generate a cumulative distribution function (CDF) for hot pixel tail sizes and a CDF for cold pixel tail sizes. The CDF shows the percentage of agricultural pixels outside the thresholds of 0.1 for cold and 1.05 for hot at different probabilities. For example, for 60% of calibrations (probability of 0.6) between 0-1% of the cold pixels are outside the calibration threshold. The CDFs developed for the hot and cold pixel tail size by Morton *et. al* is shown in Figure 3.

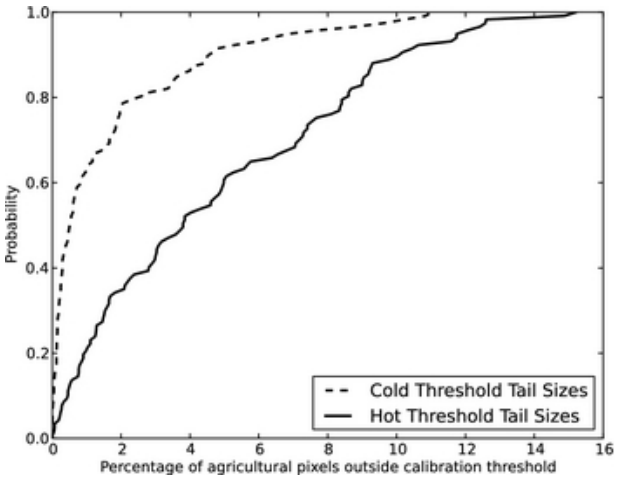

Figure 3: Cumulative distribution functions for hot and cold pixel tail size. The cold threshold is 0.1 and hot threshold is 1.05 [7].

Using these CDFs a Monte Carlo simulation was used to generate ET estimates. This procedure began by randomly selecting initial hot and cold calibration points from the final hot and cold groups developed earlier. These pixels are used to run METRIC and develop an ET_rF distribution. For each Monte Carlo integration, probabilities between 0 and 1 are randomly generated to select the target hot and cold pixel tail size. For each probability in each iteration the CDFs can be used to find the target tail size percentage. Using the ET_rF distribution generated from the random pixel selection, target ET_rF values that correspond to the target tail size percentages can be calculated. Pixels with values closest to these target ET_rF values are selected as new hot and cold pixels. These new pixels are used to run METRIC and generate a new ET_rF distribution. If tail size percentages from this new distribution are within 0.1% of the target thresholds, the Monte Carlo iteration is complete. If the tail size percentages are not within 0.1% of the targets, new ET_rF values corresponding to the target tail size percentages are calculated, new pixels are selected and METRIC is run again to develop a new ET_rF distribution. This procedure continues until the tail size percentages are within 0.1% of the targets. A flowchart of the whole iteration process is shown in Appendix A.

The automated algorithm runs 100 Monte Carlo iterations, each starting with random hot and cold pixels from the hot and cold group, and with random probability values. The idea is to use the 100 iterations to derive ET_rF distributions similar to distributions derived from multiple users for the same image. To calculate the daily ET from the iterations, the 100 ET_rF values are averaged for each pixel and multiplied by the 24 hr reference ET.

2.3 Flux Tower Systems

Flux tower data was acquired from various sources for this study. Data was collected from online flux network sites, such as OzFlux and AmeriFlux, and through personal connections. At each site one of three different types of flux tower systems was used. These systems measure and calculate sensible and latent heat fluxes in different ways. A brief description of each system will be given in this section. A description of each site is given in Chapter 3.

For all systems the soil heat flux is measured by one or more soil heat flux plates in the ground near the flux tower system. These are typically positioned between 5-10 cm below the surface. Each system also measures net radiation using a net radiometer to measure incoming and outgoing long and short wave radiation.

Eddy Covariance

Eddy covariance systems are used to directly measure the turbulent fluxes of sensible and latent heat. The system measures water vapor concentration, temperature, and high frequency wind speed in three dimensions. Water vapor and heat is transferred in the air as small and large turbulent eddies as shown in Figure 4.

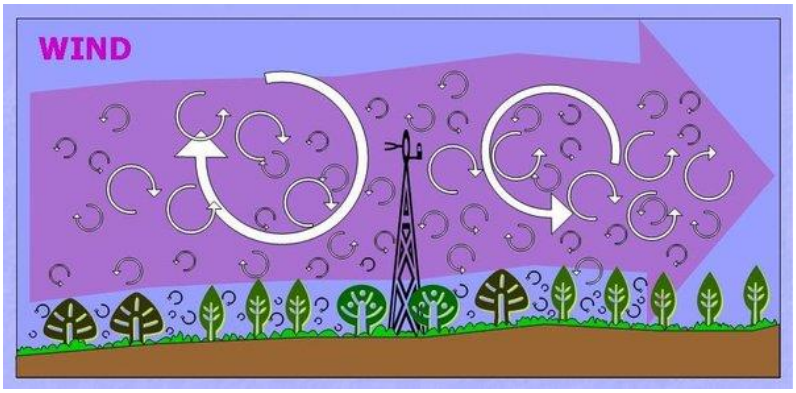

Figure 4: Eddies passing flux tower [27].

When these eddies pass the flux tower, the upward and downward transport of water vapor and heat are measured. An ultrasonic anemometers is used to measure the three wind speed components and sonic temperature. An infrared gas analyzers is used to measure fluctuations in CO_2 and H_2O concentrations. Figure 5 shows an images of the eddy covariance flux tower used at the Bear River site. Using measurements from these instruments the equations for latent and sensible heat are [28, 29]:

$$H = \rho\, C_p\, \overline{w'\, T'} \qquad (15)$$

$$\lambda E = \rho\, \lambda\, \overline{w'\, q'} \qquad (16)$$

where ρ is the density of air (kg/m^3), C_p is the specific heat of air at constant pressure (J/ (kg·K)), w' is the deviation from time averaged vertical wind speed (m/s), T' is the deviation from time averaged air temperature (K), $\overline{w'\, T'}$ is the covariance between w' and T' calculated over a certain time period, λ is the latent heat of vaporization (J/kg), q' is the specific humidity (kg/kg) and $\overline{w'\, q'}$ is the covariance between w' and q' calculated over a certain time period. Some assumptions made when calculating

fluxes with eddy covariance systems are that density fluctuations are negligible, the atmospheric fluxes are fully turbulent, the terrain where measurements are made is horizontal and uniform, and the fetch area represents the area of interest [27]. Since all energy balance components are measured independently with eddy covariance systems, there is often a lack of energy balance closure. Several possible reasons for lack of closure and the methods used in this study to adjust for closure are discussed in Section 2.4.

Several of the flux tower data sets used in this study came from one sensor eddy covariance systems. These systems do not have an infrared gas analyzer, hence they cannot provide a direct latent heat flux measurement. Sensible heat is measured, as mentioned above, with an ultrasonic anemometer. For a one sensor eddy covariance system the latent heat flux is calculated as a residual of the other energy balance fluxes.

Figure 5: Eddy covariance flux tower at Bear River site in Utah [30].

Bowen Ratio-Energy Balance Method

The Bowen ratio-energy balance method is an indirect way to measure evaporation from the earth's surface. The Bowen ratio is defined as the ratio between the sensible heat flux and the latent heat flux. It can also be calculated as the ratio between the change in actual air temperature and the change in actual vapor pressure over two measurement levels Eq. (17) [31]. With the Bowen ratio calculation and separate measurements of net radiation and soil heat flux, Eqs. (18) and (19) can be used to calculate latent and sensible heat fluxes respectively.

$$\beta = \frac{H}{\lambda E} = \gamma \frac{\Delta T}{\Delta e} \quad (17)$$

$$\lambda E = \frac{R_n - G}{1 + \beta} \quad (18)$$

$$H = \frac{\beta\,(R_n - G)}{1 + \beta} \quad (19)$$

where β is the Bowen ratio, γ is the psychrometric constant (kPa/K), ΔT is the gradient of air temperature over a certain height (K), and Δe is the gradient of the vapor pressure over a certain height (kPa). The Bowen ratio method can calculate latent and sensible heat fluxes using less expensive

equipment than eddy covariance systems. Temperature and vapor pressure gradient values can be calculated using two temperature and vapor pressure sensors at different heights. The method assumes that the fluxes are one-dimensional and that there is no horizontal gradient. It is also assumed that the two measurement heights are in a sublayer where fluxes are constant with height [32].

Surface Renewal

Surface renewal systems use high frequency air temperature data measured with thermocouples to estimate the sensible heat flux. In 1991 Paw U and Brunet introduced the surface renewal method for measuring sensible heat flux densities [33]. Air parcels transfer heat to and from the canopy, causing the parcels to increase or decrease in temperature. These temperature changes in time can be modeled as ramps. Using the ramp amplitude and total duration, the sensible heat flux can be estimated [34]. Sensible heat fluxes using this method must be calibrated using sonic anemometer sensible heat measurements to determine the surface renewal weighting factor. Similar to the other flux tower systems used in this study, soil heat flux is measured by soil heat flux plates and net radiation is measured by a net radiometer. Latent heat fluxes are calculated as the residual using the surface energy balance.

2.4 Closure of Eddy Covariance Flux Tower Data

Energy balance flux components measured using eddy covariance (EC) systems often have a lack of closure of the surface energy balance. This lack of closure occurs because each surface energy flux is measured independently in eddy covariance systems and these measurements are not always consistent with the principle of the conservation of energy. Previous research indicates several explanations for the lack of closure in EC systems including: instrument measurement errors and malfunctions, difference in source areas for different components, neglecting energy stored in top soil or tree canopies, corrections made when processing data, neglected energy sinks, and averaging components in a certain time period resulting in the loss of low and or high frequency turbulent heat fluctuations [35]. A study of 22 eddy covariance sites showed a mean imbalance in closure of 20% [36]. All components have error associated with them, however, measurements of sensible and latent heat fluxes have been found to be underestimated by around 10-30% [36]. Net radiation is generally considered the most accurate measurement. Measurement errors are also associated with the soil heat flux, however, this flux typically only accounts for a small portion of the net radiation so errors from this flux are not one of the main causes for lack of closure.

The closure bias for each overpass day selected was calculated using Eq. (20). Previous research has indicated that days with closure values smaller than 0.7 measurements are less trustworthy because of the large lack of closure from unknown causes. In this study days with closure values smaller than 0.65 were not used for analysis. The majority of the days selected from eddy covariance sites had closure values greater than 0.7. However, due to the lack of cloud free days during the period with available data, a few days with closure values between 0.65 and 0.7 were selected from several sites.

$$Closure = \frac{H + \lambda E}{R_n - G} \qquad (20)$$

Closure values were only used as a criterion for selecting days from two sensor eddy covariance sites. Due to the lack of direct latent heat measurements from one sensor eddy covariance sites, closure cannot be calculated for these days.

In this study, daily flux data from eddy covariance sites was corrected for closure by calculating latent heat as the residual and by adjusting for closure with the Bowen ratio. Daily ET values were calculated from the latent heat estimations resulting from both of these methods and from the direct latent heat measurements.

Latent Heat as Residual

One method of closure is to calculate the latent heat flux as a residual of the other fluxes instead of using the direct latent heat measurements. Latent heat flux measurements are not used with this method because some researchers believe that eddy covariance systems are more accurate at measuring H than λE [37]. The residual latent heat flux is calculated as:

$$\lambda E = R_n - H - G \quad (21)$$

Since latent heat fluxes are typically underestimated by eddy covariance systems, using the residual results in larger latent heat flux values which results in higher daily ET values. All comparisons between flux tower data and the modeled results from SEBAL3.0 and EEFlux have been completed using the residual latent heat values.

Bowen Ratio Closure

The second measure of closure used was to adjust for closure using the measured Bowen ratio. This method assumes that eddy covariance instruments accurately measure the Bowen ratio. The daytime Bowen ratios and the daytime residual energy flux are calculated. λE and H are both adjusted to account for the residual while preserving the original Bowen ratio. Since any daytime energy balance residual gets divided between both λE and H, daily ET values typically are larger than values calculated using the directly measured λE, but smaller than daily ET values calculated using λE as a residual since all the residual is divided with Bowen ratio closure.

2.5 Footprints

The measurements of sensible heat flux using a sonic anemometer and latent heat flux using an infrared gas analyzer represent the conditions in the upwind area of the flux tower called the footprint. The shape and length of a flux footprint depend on the measuring height, wind speed, surface roughness, and atmospheric stability conditions. Determining the footprint area of the measurement data is important in order for values from the modeled data to represent the same area, allowing for comparison. There are footprint models used to estimate the size and shape of the upwind area influencing the sensible and latent heat measurements, however, for this study a standard footprint was used for all sites. For each simulation day, the direction of the footprint was adjusted to be in the upwind direction from the site. The flux tower measured wind directions were categorized as north, east, south or west depending on their nearest direction. The standard footprints length was 10 pixels (300 m) in the upwind direction and its width increased in increments from 1 pixel (30 m), at the flux tower site, to 5 pixels (150 m), at the furthest upwind direction. Pixel values in this footprint area were averaged to determine modeled outputs of daily ET and instantaneous sensible heat flux. Measurements of net radiation and soil heat flux are point measurements, which represent a much smaller area than the latent and sensible heat measurement footprint. The modeled outputs for net radiation and soil heat flux values were obtained from the modeled pixel at the location of the flux tower.

Since the flux tower instrument height varied per site, the use of a standard footprint means the footprint averaged values could include values from outside the flux tower measurement area or exclude area that was measured by the flux tower. In a homogenous landscape the effects from this misrepresented area would be minimal due to ET and sensible heat flux being relatively close over the whole area. However, there were several sites where the footprint area was not homogenous, which could affect measurements. For example, one flux tower site was in an irrigated field surrounded by a barren dry landscape. When the prevailing wind direction was from the west or east the footprint fell outside of this irrigated field and averages included values from the surrounding landscape. If the standard footprint used in this study was larger than the actual footprint area for these days at this site, than the exclusion of values from the surrounding area could lower modeled outputs.

3 Sites

Eighteen flux tower sites were selected as study sites as shown in Figure 6. These sites were selected to represent various climatic conditions and land cover types. Table 1 displays site locations and an overview of site characteristics. Sites were split into two sets: Set 1 and Set 2. Set 1 was used for initial model runs and for calibration of the hot and cold pixel constant. Set 2 was used for validation of the new hot and cold pixel constant combination. These hot and cold constants are used in Eqs. (7) and (8).

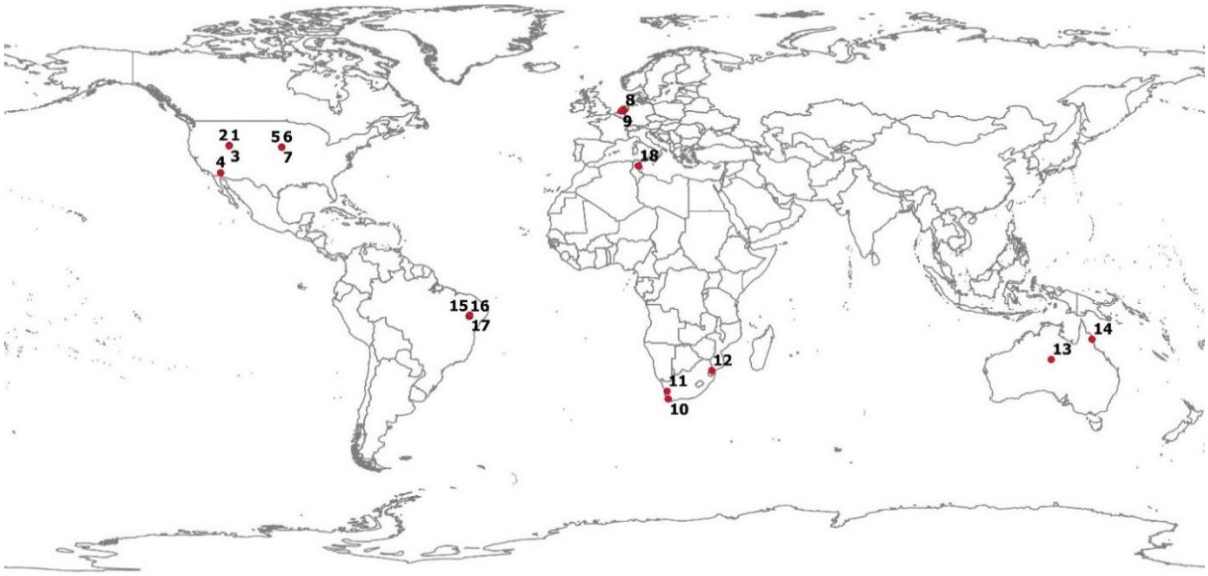

Figure 6: Location of flux towers sites selected for this study.

Table 1: Overview of flux tower sites selected for this study including site ID, site name, site coordinates, type of flux tower system, vegetation type and whether the site is irrigated. Set 1 is used for initial run and calibration and Set 2 is used for validation.

Site #	Site ID	Site Name	Country	Latitude	Longitude	System	Vegetation Type	Irrigation
SET 1								
1	BR-C	Bear River-Corn	USA	41.6327	-112.1604	Eddy Covariance	Corn	X
2	BR-W	Bear River- Wheat	USA	41.6363	-112.1606	Eddy Covariance	Wheat	X
3	BR-O	Bear River- Onion	USA	41.5054	-112.1732	Eddy Covariance	Onion	X
4	PV	Palo Verde	USA	33.4690	-114.7147	Bowen Ratio	Alfalfa	X
5	Ne-1	Mead- Irr. Maize	USA	41.1651	-96.4766	Eddy Covariance	Maize	X
6	Ne-2	Mead- Irr. Maize Soybean	USA	41.1649	-96.4701	Eddy Covariance	Maize-soybean rotation	X
7	Ne-3	Mead- Rain-fed Maize Soybean	USA	41.1797	-96.4397	Eddy Covariance	Maize-soybean rotation	
8	LB	Loobos	NLD	52.1679	5.7440	Eddy Covariance	Scots Pine	
9	CB	Cabauw	NLD	51.9703	4.9262	Eddy Covariance	Open Pasture (Grassland)	
SET 2								
10	VL	Vergelegen	ZAF	-34.0813	18.9016	1 Sensor EC	Grapes	X
11	S3	Kapel	ZAF	-31.7726	18.5788	1 Sensor EC	Grapes	X
12	KM	Komati	ZAF	-25.5953	31.8922	Surface Renewal	Sugarcane	X
13	AS	Alice Springs	AUS	-22.2838	133.2493	Eddy Covariance	Mulga	
14	CW	Cow Bay	AUS	-16.2382	145.4271	1 Sensor EC	Tropical rainforest	
15	BR-TG	São Francisco River Basin- TG	BRA	-9.3113	-40.3748	Bowen Ratio	Table Grape	X
16	BR-M	São Francisco River Basin- M	BRA	-9.3756	-40.5650	Eddy Covariance	Mango	X
17	BR-C	São Francisco River Basin- C	BRA	-9.0585	-40.3292	Eddy Covariance	Caatinga	
18	TN	Tunisia	TUN	35.5591	9.94032	Eddy Covariance	Wheat	

Bear River

The Bear River sites are located in the United States in Northern Utah. This site has three eddy covariance flux towers located in the 29,764 ha Bear River Canal Company irrigation district. The flux towers are all located in irrigated fields: one in a corn field, one in a wheat field and one in an onion field. Winds in this area come predominantly from the southwest so each flux tower was located in the northeast corner of the field. These flux tower sites were operated by Utah State University and data was acquired for the 2013 growing season through a personal connection. Five Landsat 8 overpass days were selected between July and September 2013. Meteorological data was obtained from a local meteorological station in Tremonton, UT operated by the Utah Climate Center.

The Bear River site is located in a semi-arid climate. The area has very warm and dry summers with cold and moderately snowy winters. Precipitation is heaviest in the spring during April, March and May.

Palo Verde

The Palo Verde site is located in the United States in southern California near the California/Arizona border. The site has one Bowen ratio system located in the 48,950 ha Palo Verde Irrigation District. The crop cover in the district is 90 percent alfalfa, 5 percent cotton and the remaining 5 percent grains and mixed vegetables [38]. The Bowen ratio flux tower is located in the center of an irrigated alfalfa field. This flux tower was operated by Utah State University and data was acquired through a personal connection for 2008. Eleven Landsat 5 and four Landsat 7 overpass days between January and September 2008 were selected for this study. Meteorological data was obtained from a local meteorological station in Ripley, UT operated by the California Department of Natural Resources.

The Palo Verde site is located in a dry arid climate. The irrigation district area is surrounded by the Colorado Desert. The area has very hot summers and mild winters. On average there is under 120 mm of precipitation per year with rainy periods in the late summer and winter.

Mead, NE

The Mead sites are located in the Midwestern United States in eastern Nebraska. The site has three eddy covariance flux towers located in a flat plain cropland area. Mead Site 1 is in a continuous maize field with a center pivot irrigation system. Mead Site 2 is in a maize-soybean rotation field with a center pivot irrigation system. Mead Site 3 is in a maize-soybean rotation field with no irrigation. All three fields are located within 1.6 km of each other. Data for the time period from January 2001 to May 2013 was acquired online from Ameriflux. The sites are operated by the University of Nebraska-Lincoln. Eight Landsat 7 overpass days in 2012 were selected for this study. Meteorological data was obtained from a local weather station in Mead, NE operated by the High Plains Regional Climate Center.

The Mead site is located in a humid continental climate. The area experiences hot, humid summers with cold winters. On average the area receives approximately 780 mm of annual precipitation. Precipitation is heaviest during the summer months and in the winter precipitation is often in the form of snow.

Loobos

The Loobos site is located in the middle of the Netherlands. The site has one eddy covariance flux tower located in a forested area. The area within a 500 m radius around the flux tower is composed of 89% Scots pine, 7.5% black pine, birch, Douglass fir or oak and 3.5% open area covered by grass or heather [39]. The site has been operated by Alterra since 1994. Data is available from 1996 to 2015 on the climate exchange website operated by Alterra [39]. Two Landsat 8, eight Landsat 7 and one Landsat 5 overpass days between April 2011 and May 2013 were selected for this study. Meteorological data was obtained from a local weather station operated by the Royal Netherlands Meteorological Institute.

The Loobos site has a temperate marine climate. The area experiences cool summers and mild winters. The area receives on average 770 mm of annual precipitation distributed relatively evenly throughout the year.

Cabauw

The Cabauw site is located in the middle of the Netherlands. The site has one eddy covariance flux tower. The dominant vegetation cover in the surrounding area is grassland. The site has been operated by Alterra since 2001. Data is currently available from 2001 to April 2016 on the Cabauw experimental site for atmospheric research website (Cesar) [40]. Four Landsat 8 and three Landsat 7 overpass days in the period of September 2013 to March 2014 were selected for this study. Meteorological data was obtained from a local weather station operated by the Royal Netherlands Meteorological Institute. The climate at the Cabauw site is similar to the climate at the Loobos site.

Vergelegen

The Vergelegen site is located on the coast in southwestern South Africa. The site has a one sensor eddy covariance flux tower. This flux tower does not have an IRGA (infrared gas analyzer). The flux tower is located in the center of an irrigated Cabernet Sauvignon grape vineyard plot. This site is operated by Caren Jarmain (University of KwaZulu-Natal) and data was acquired for July 2013 to May 2016 through a personal connection. Five Landsat 8 and four Landsat 7 overpass days in 2015 were selected for this study. Meteorological data was obtained from a weather station in Somerset West, a nearby town.

The Vergelegen site has a Mediterranean climate. The area experiences dry, warm summers and mild, wet winters. Precipitation is heaviest in the late fall and winter months from April to August.

Kapel

The Kapel site is located on the western coast of South Africa. This site has a one sensor eddy covariance flux tower. The flux tower is also located in the center of an irrigated Cabernet Sauvignon grape vineyard plot and operated by Caren Jarmain (University of KwaZulu-Natal). The irrigated plot of land is surrounded on three sides by a barren/natural vegetation area which is very dry in summer. Data was acquired for December 2013 to July 2016 through a personal connection. Eleven Landsat 8 and six Landsat 7 overpass days were selected between August 2014 and July 2016. Meteorological data was obtained from a weather station in Klawer, a nearby town.

The Kapel site has a semi-arid climate. The area has very hot and dry summers with mild winters. Annual rainfall is around 158 mm with the heaviest rainfall in winter months (May to August) and very little rainfall in December, January and February.

Komati

The Komati site is located in western South Africa north of Swaziland near the South Africa/Mozambique border. The site has one surface renewal flux tower in an irrigated sugarcane field. This site is operated by Caren Jarmain (University of KwaZulu-Natal). Data was acquired for December 2011 to December 2012 through a personal connection. There were only four cloud free Landsat 7 overpass days in the data time period. These days were selected for this study. Daily meteorological data was obtained from the Komati automatic weather station operated by the South African Sugarcane Research Institute (SASRI). Instantaneous meteorological data for the time of satellite overpass was obtained from GLDAS using the three hour data that included the overpass time.

The Komati site has a temperate climate with dry winters and wet, hot summers. Unlike the other South Africa sites, this site receives most of its rainfall in the summer months of December to February. Winters are very mild with mid-day temperatures averaging around 25 °C.

Alice Springs

The Alice Springs site is located in central Australia in the Northern Territory. The site has one eddy covariance flux tower in a shrubland area. The land cover is predominantly Mulga Acacia trees with a canopy at around 6.5 m [41]. The site is supported by the Terrestrial Ecosystem Research Network (TERN) and operated by the University of Technology Sydney. Data was available from 2010 to 2015 on the Oz Flux website. Five Landsat 8 and four Landsat 7 overpass days between November 2013 and July 2014 were selected for this study. Meteorological data was acquired from Ti Tree, a nearby flux site with available meteorological measurements of the required data.

The Alice Springs site is in a hot semi-arid climate. Summers are very hot and winters are mild but can have cool nighttime temperatures which is partially caused by the site's high elevation (606 m above sea level). The mean annual precipitation is 306 mm but can vary significantly from year to year with recent years ranging from 100 mm to 750 mm.

Cow Bay

The Cow Bay site is located on the northern east coast of Australia in Queensland. The site has a one sensor eddy covariance flux tower in a lowland tropical rainforest. The forest is type 1a, complex mesophyll vine forest with a canopy height averaging about 25m [42]. The site is supported by the Daintree Discovery Centre and TERN, and operated by James Cook University (Cairns Campus). Data was available on Oz Flux from 2009 to 2015, however, soil heat flux data was missing for all years except 2015. There were also a limited number of cloud free days in the data time period which resulted in only one Landsat 8 and two Landsat 7 scenes that could be selected. Meteorological data was acquired from Cape Tribulation, a nearby flux site with available meteorological measurements of the required data.

The Cow Bay site is located in a tropical monsoon climate. Annual average precipitation is approximately 4250 mm with heaviest rainfall in the wet season from January to April. Year round mean daily temperatures range between 21°C and 26°C from winter to summer.

São Francisco River Basin

The São Francisco River Basin sites are located in eastern Brazil in the State of Pernambuco. This site has four flux towers: one Bowen ratio system in an irrigated wine grape plot, one Bowen ratio system in an irrigated table grape plot, one eddy covariance system in an irrigated mango plot and one eddy covariance system in a natural caatinga landscape. The sites were managed by A.H. De C. Teixeira from the Brazilian Agricultural Research Corporation (Embrapa). Five Landsat 5 overpass days were selected between 2003 and 2005. Flux tower measurements for these days were acquired through a personal connection. Daily average meteorological data from local agro-meteorological stations were acquired from a previous study using the flux data [43].

The São Francisco River Basin has a semi-arid climate. The entire year has hot temperatures with monthly averages varying by only 3.7°C. The area receives on average an annual 600 mm of precipitation, with a rainy season from December to May.

Tunisia

The Tunisia site is located in northeastern Tunisia. The site has one eddy covariance flux tower in a rain-fed wheat field. The flux tower was managed by Gilles Boulet from the Centre d'Etudes Spatiales de la BIOsphère (CESBIO). Thirty minute energy balance flux components were acquired for five Landsat 7 overpass days through a personal connection. Daily meteorological data was obtained from GLDAS and instantaneous data was acquired from the site.

The Tunisia site is in a semi-arid climate. The average annual precipitation is about 300 mm with heaviest precipitation in the fall. Summers have a daily mean temperature of 28°C while winters have a daily mean temperature of 12°C.

4 Results and Analysis

4.1 Eddy Covariance Flux Tower Closure

As mentioned in Section 2.4, eddy covariance systems measure all flux components independently which often results in a lack of closure of the surface energy balance. Latent heat flux values and daily ET rates were calculated for all eddy covariance sites using two methods of closure: Bowen ratio closure and latent heat as residual. Eddy covariance flux measurements closed using the latent heat flux as the residual will be used for all comparisons with modeled data in this study.

Overpass days were only selected if the value for closure was above 0.65. For the days in this study the average closure was 0.81 and the maximum closure of all selected days 0.95. For the days selected in this study residual energy fluxes ranged from 128 W/m^2 to 3487 W/m^2. Latent heat flux values closed with the Bowen ratio were on average 26% larger than direct latent heat measurements. The maximum increase was 68% and the minimum increase was 5%. Latent heat flux values closed using latent heat as the residual were on average 70% larger than direct latent heat measurements. The maximum increase was 9% and the minimum increase was 387%. These very large increases seen in the latent heat as residual closures, result from days at the Alice Springs and the Brazil site with a natural landscape. Both of these areas have very small latent heat fluxes and very large sensible heat fluxes. However, using latent heat as a residual assigns all the residual as latent heat resulting in large increases from the direct measurements. These days have small direct measurements for latent heat values due to the dry landscape with no irrigation. These sites also have the largest difference between the Bowen ratio closed latent heat fluxes and the residual latent heat fluxes. The large difference between the two methods of closures for these sites exists because of the large Bowen ratios for the dry environments. With a large Bowen Ratio the majority of the residual is assigned to sensible heat flux and only a small portion of the residual is added to the latent heat flux. These comparisons show the error that exists in eddy covariance field measurements and how the method of closure affects the resulting latent heat flux values.

4.2 First Data Set Comparison

From the first set of flux towers, 63 Landsat scenes from cloud free overpass days were selected for comparison of SEBAL3.0 results and EEFlux results with flux tower measurements. An overview of the selected days per site and the meteorological inputs used for the SEBAL3.0 model Set 1 runs can be found in Appendix B. Figure 7 and Figure 8 show the comparison of daily ET rates estimated by SEBAL and EEFlux respectively to ground flux tower measurements for Set 1 sites. All comparison figures categorize results by site because sites had different flux tower systems.

For all sites combined, SEBAL3.0 performed better than EEFlux for the first set of flux tower sites. SEBAL3.0 data had a root mean squared error (RMSE) of 2.48 mm/d and EEFlux had an RMSE of 6.24 mm/d excluding 4 data points that had unreasonable daily ET values larger than 1000 mm/d and smaller than -50 mm/d. The RMSE values per site for both SEBAL3.0 and EEFlux are listed in Table 2.

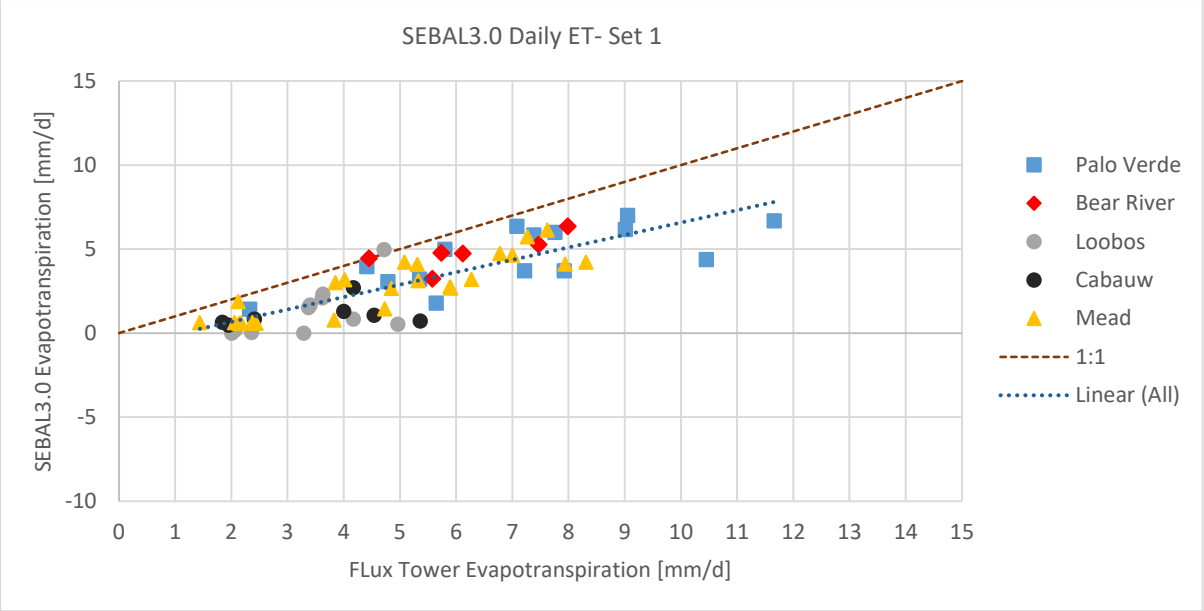

Figure 7: Comparison of daily evapotranspiration rates estimated from SEBAL3.0 with flux tower measurements for Set 1 sites.

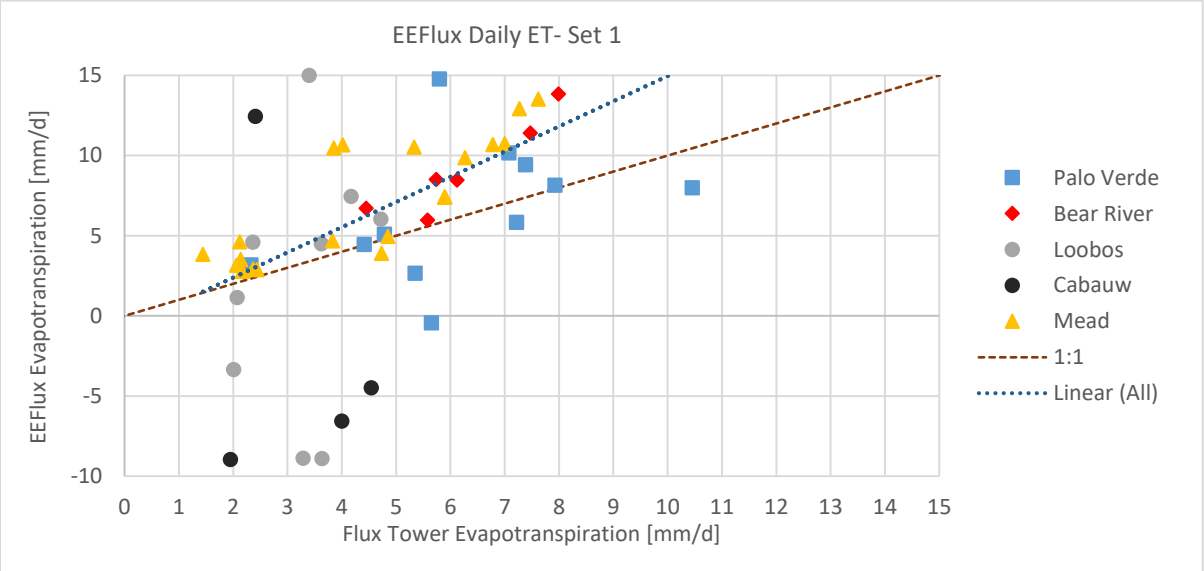

Figure 8: Comparison of daily evapotranspiration rates estimated from EEFlux with flux tower measurements for Set 1 sites.

EEFlux results show much more scatter than the SEBAL3.0 results with especially large deviations for some of the days with lower daily ET values. The days with the unreasonable values that were removed from analysis and the days with the largest deviation from the 1:1 line were overpass days used for the Netherlands sites. Excluding the Netherlands sites from Set 1 sites and leaving only the United States sites results in an improved RMSE of 4.92mm/d. A presentation of EEFlux stated that the model was more refined for areas in the continental United States [15]. Data inputs, such as weather data, are from a different source for the United States than for the rest of the world. There is a possibility that the data sources used for the United States, which were developed specifically for the country, provide more accurate data than global data sources which are used for all other countries. The METRIC model, which EEFlux is based on, has typically been used for estimates in agricultural areas. The non-

agriculture fields of the Netherlands sites could also be a possible explanation for the poor performance of these sites. The Netherlands sites had a RMSE 9.21 mm/d.

SEBAL3.0 results show a systematic underestimation of daily ET estimates. Lower ET rates are underestimated by smaller rates but larger percentages than the larger ET rates. There were no results from SEBAL3.0 with unreasonable values. RMSE's per site ranged from 1.69 mm/d for Bear River to 2.99 mm/d for Palo Verde. Unlike EEFlux, SEBAL3.0 results did not show a large difference between the performance of the model in estimating daily ET rates for the Netherlands and for the United States. The Netherlands sites had an RMSE of 2.52 mm/d and the United States sites had a RMSE of 2.46 mm/d. Compared to the much larger performance difference between the two countries from the EEFlux results, it can be concluded from Set 1 results that SEBAL3.0 is more applicable for different locations. Results from the additional Set 2 locations will be discussed in Section 4.4.

Table 2: RMSE's for both models per site for Set 1 sites.

Site	Number of Overpass days	SEBAL3.0 RMSE [mm/d]	EEFlux RMSE [mm/d]
Bear River	6	1.6	2.9
Palo Verde	15	3.0	5.0
Mead	24	2.3	5.3
Loobos	11	2.4	7.4
Cabauw	7	2.7	11.8

Since SEBAL3.0 outputs results for energy balance flux components as well as daily ET results, further analysis was completed to investigate which components contributed to the systematic underestimation. Figure 9 shows the SEBAL3.0 instantaneous evaporative fraction and daily averaged net radiation results compared to flux tower measurements. Figure 10 shows the SEBAL3.0 instantaneous sensible heat flux results compared to flux tower measurements. Other SEBAL3.0 instantaneous energy flux components comparisons for Set 1 can be found in Appendix B.

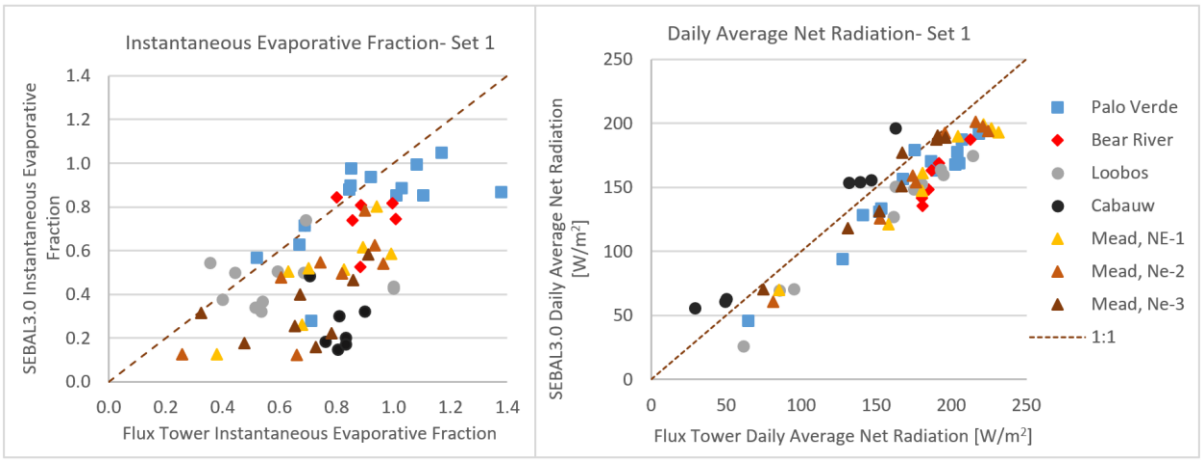

Figure 9: Comparison of SEBAL3.0 instantaneous evaporative fraction and daily averaged net radiation results with flux tower measurements for Set 1 sites.

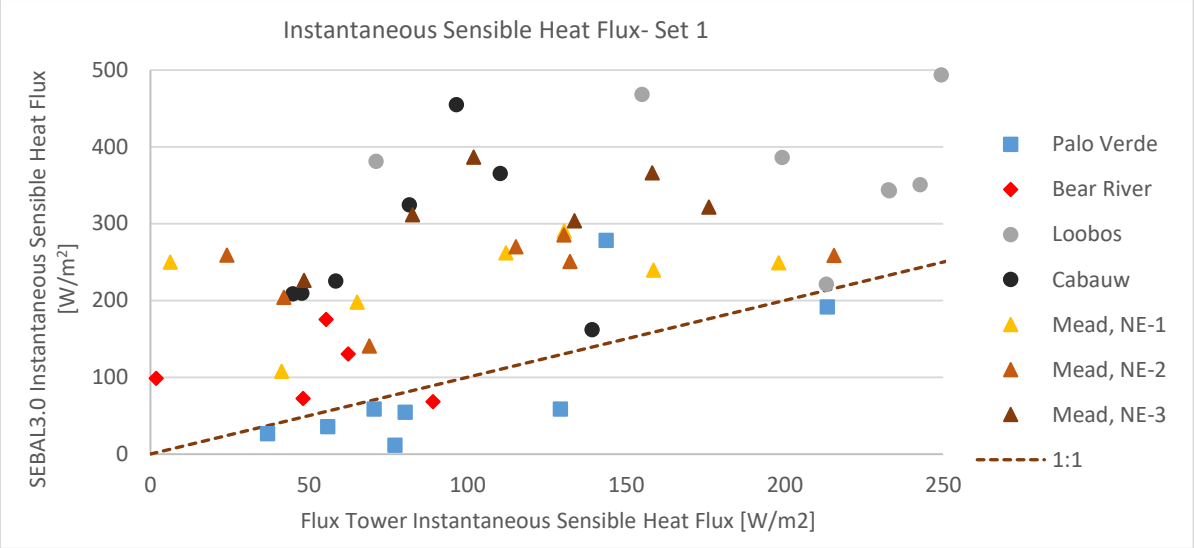

Figure 10: Comparison of SEBAL3.0 instantaneous sensible heat flux results with flux tower measurements for Set 1 sites.

The daily averaged net radiation results show an underestimation of results for all sites except Cabauw which has a slight overestimation. The RMSE of all Set 1 sites combined is 26.11 W/m^2. Daily averaged net radiation is used in Eq. (11) to upscale instantaneous values to daily ET. As a result of this calculation, the errors in the daily net radiation are transferred to the estimates of daily ET. Results of the instantaneous evaporative fraction also show an underestimation of SEBAL3.0 results for most days. Instantaneous evaporative fractions are underestimated due to the underestimation of daily averaged net radiation and the estimations for sensible heat fluxes. Results for the instantaneous sensible heat flux show much more scatter than the daily averaged net radiation results. Results were systematically overestimated by SEBAL3.0 with overestimations up to 358 W/m^2 and a RMSE of 166 W/m^2 for all Set 1 sites. Since latent heat is calculated as the residual, large overestimations of sensible heat fluxes will result in lower latent heat fluxes and lower daily ET rates. These sensible heat flux results are affected by the pixel selection procedure that was automated to develop SEBAL3.0. The next section gives the results of the hot and cold pixel constant calibration procedure performed to improve the sensible heat flux results.

4.3 Set 1 Pixel Selection Constant Calibration Results

Based on the results from the first data set comparison, which show a systematic overestimation of the sensible heat estimates, a calibration of the hot and cold pixel surface temperature constant, described in Section 2.1, was performed. The goal was to find the optimum pixel combination to improve model performance. Two overpass days from Set 1 sites Loobos, Mead, and Palo Verde were used for the calibration to test the 15 hot and cold pixel constant combinations. Figure 11 and Figure 12 show the results of the pixel constant estimates for instantaneous sensible heat flux and daily evapotranspiration respectively for the two irrigated Mead sites. Results from the calibration runs for the other two sites are shown in Appendix C. "H" is used to indicate the hot constant and "C" is used to indicate the cold constant.

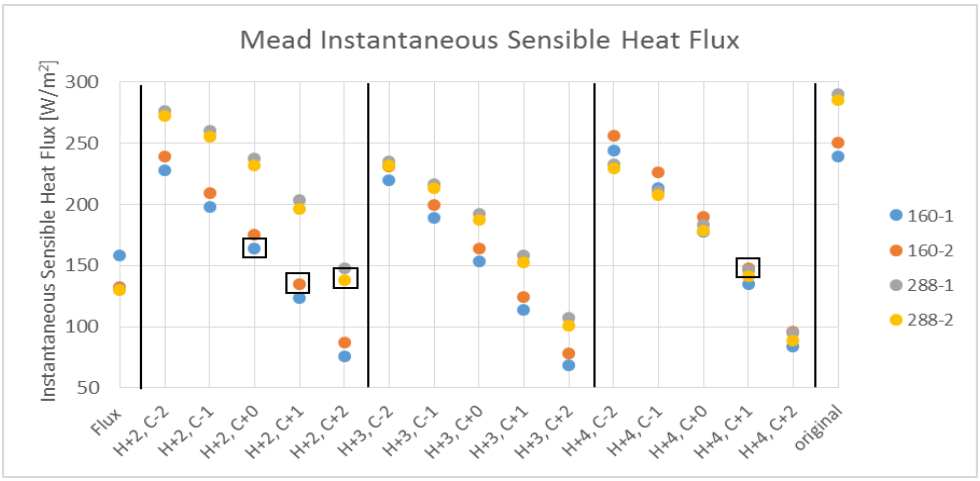

Figure 11: Instantaneous sensible heat flux values for all 15 pixel constant combinations for days 160 and 288 at Mead-1 and Mead-2 sites. Flux tower sensible heat measurements are shown on the left side and original SEBAL3.0 estimates before calibration procedure are shown on the right side. Boxes indicate the best pixel combination per site per day.

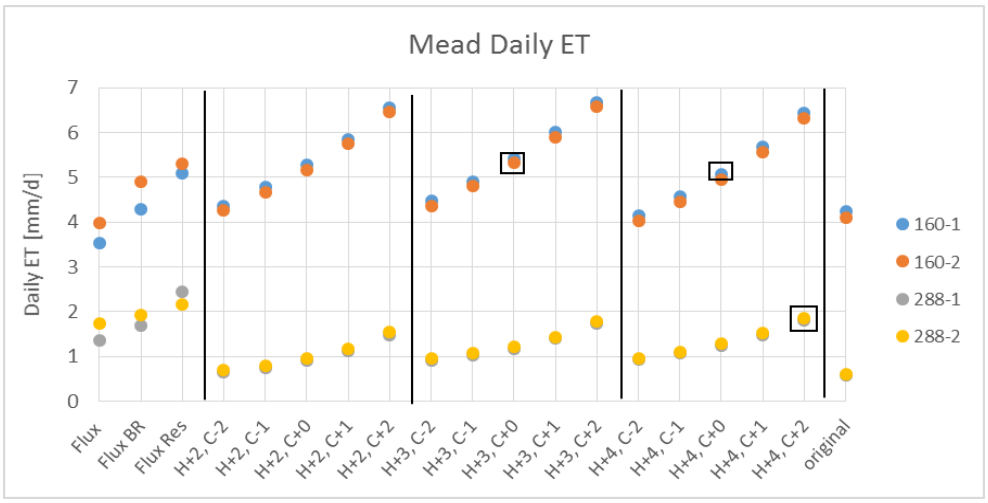

Figure 12: Daily evapotranspiration values for all 15 pixel constant combinations for days 160 and 288 at Mead-1 and Mead-2 sites. Directly measured and adjusted for closure flux tower measurements are shown on the left side. "Flux" is the daily ET calculated from direct λE measurements. "Flux BR" is daily ET calculated from λE measurements closed with the Bowen Ratio and "Flux Res" is daily ET calculated from λE measurements closed using λE as the residual. Results from original pixel constants before calibration shown on the right side. Boxes indicate the best pixel combination per site per day based on the closest combination to the "Flux Res" measurement data which is closed using the latent heat as the residual.

Pixel adjustment results for both instantaneous sensible heat flux and daily evapotranspiration show a larger impact from the adjustment of the cold pixel constant than from adjustment of the hot pixel constant. Mead daily ET results show a maximum increase in ET of 2.3 mm/d from adjusting the cold pixel constant and only 0.37 mm/d from adjusting the hot pixel constant. For the Mead results this large impact of the cold pixel constant could result from the flux tower being located in an irrigated field with surface temperatures closer to the cold pixel anchor than the hot pixel anchor. This would cause the larger influence from the cold pixel constant in the irrigated area and in surrounding dry land, the hot pixel constant would have a larger influence. The Loobos site, which is a non-irrigated forest, has a larger influence from the hot pixel constant than the Mead site. However, the influence of the cold pixel is still larger than the hot pixel, hence results show daily ET rates are still more sensitive to adjustment of the cold pixel constant. At Loobos the maximum increase in ET from adjustment to the cold pixel

constant was 1.81 mm/d and a maximum increase of 1.07 mm/d from adjustment to the hot pixel constant.

The best pixel combination per site and per day based on the daily ET was selected as the pixel constant combination with results closest to the flux tower daily ET closed using latent heat as the residual for the eddy covariance sites. Flux tower data of ET from direct latent heat measurements and ET values from closure with the Bowen ratio are also presented in Figure 12. When calibrating the pixel constant selection with daily ET data, optimum results will change based on the method of closure used.

The results of the best two pixel constant combinations for calibrating for instantaneous sensible heat flux values can be seen in Table 3 and for calibrating for daily ET can be seen in Table 4.

Table 3: Calibration results for instantaneous sensible heat flux estimates. Best pixel and second best pixel combinations for each day and each site shown.

	H+2					H+3					H+4				
	C-2	C-1	C+0	C+1	C+2	C-2	C-1	C+0	C+1	C+2	C-2	C-1	C+0	C+1	C+2
Loobos 121			2			1									
Loobos 273	1	2													
Mead 160-1			1					2							
Mead 160-2				1					2						
Mead 288-1					2									1	
Mead 288-2					1									2	
Palo Verde 83			2				1								
Palo Verde 139			1					2							

Table 4: Calibration results for daily evapotranspiration estimates. Best pixel and second best pixel combinations for each day and each site shown.

	H+2					H+3					H+4				
	C-2	C-1	C+0	C+1	C+2	C-2	C-1	C+0	C+1	C+2	C-2	C-1	C+0	C+1	C+2
Loobos 121				1							2				
Loobos 273			2									1			
Mead 160-1							2						1		
Mead 160-2			2					1							
Mead 288-1										2					1
Mead 288-2										2					1
Palo Verde 83								1	2						
Palo Verde 139				2											1

The results showed no clearly optimum constant combination. The optimum pixel constant combination varies depending on whether results are calibrated for instantaneous sensible heat flux or daily ET. This difference is due to the other energy balance components in addition to the sensible heat flux that affect daily ET rates. The results indicate that there is a temporal variation in optimum results. When looking at the sites separately, the optimum pixel combination varies depending on the day. There is also spatial variation in the optimum results. This spatial variation is not only evident when looking at sites located in different states or countries, but also evident at sites with multiple flux towers within a short distance of one another. The two flux towers at the Mead site, used for the pixel constant calibration, are less than 600 m apart from each other. According to the calibration results different constant combinations should be used for these two sites on the same day even though they are very close to each other.

The majority of the optimum pixel constant combinations per day and per site are in the H+2 category for instantaneous sensible heat flux. For daily ET the majority of the optimum pixel constant combinations are in the H+4 combination. Although there is no clear optimum for either the hot or cold constant, there is less of a majority for a particular constant when evaluating results for the more influential cold pixel constant. A majority of the optimum pixel constant combinations are in the C+0 category for the instantaneous sensible heat results. For daily ET results, the majority of optimum results are in either the C+0 or C+2 categories. Since the results did not show a clear optimum combination for either daily ET or for instantaneous sensible heat flux, new constants were selected for further analysis based on the instantaneous sensible heat results. The constants directly affect the surface temperatures used in the sensible heat calibration. The constants affect daily ET results as well, but other factors also influence these results. The final constant combination was selected as +2 for the hot pixel constant and +0 for the cold pixel constant. This combination was based on the hot and cold constants which had the majority of optimum constant combinations.

4.4 Second Data Set Comparison

From the second set of flux towers, 53 Landsat scenes from cloud free overpass days were selected for comparison of SEBAL3.0 results, with adjusted hot and cold pixel surface temperature constants, and EEFlux results with flux tower measurements. An overview of the selected days per site and the meteorological inputs used for the SEBAL3.0 model Set 2 runs can be found in Appendix D. Figure 13 and Figure 14 show the comparison of daily ET rates estimated by SEBAL3.0 and EEFlux respectively to ground flux tower measurements for Set 2 sites.

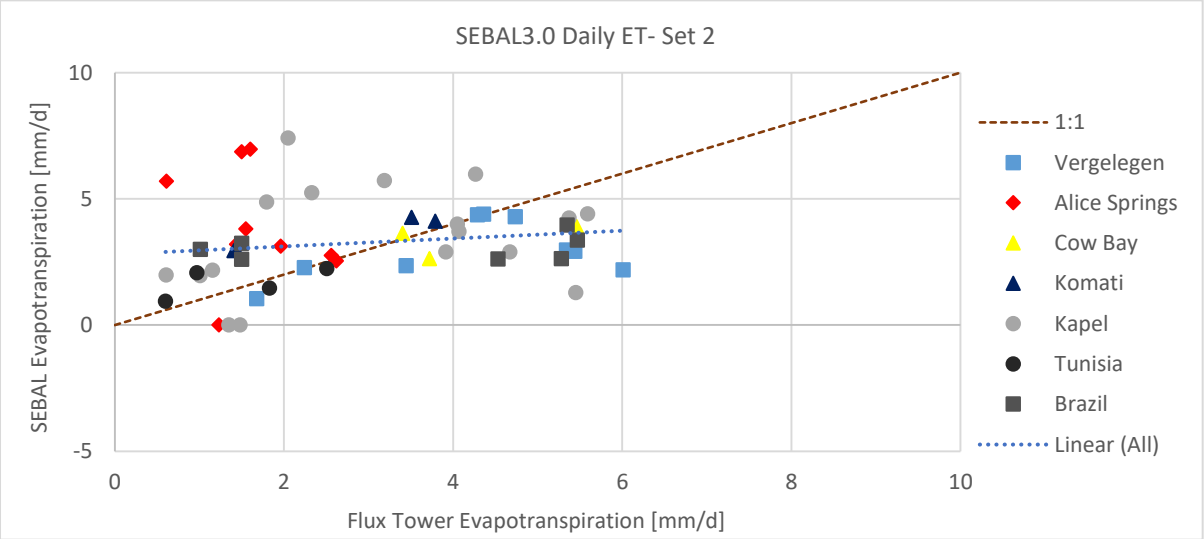

Figure 13: Comparison of daily evapotranspiration rates estimated from SEBAL3.0 with flux tower measurements for Set 2 sites.

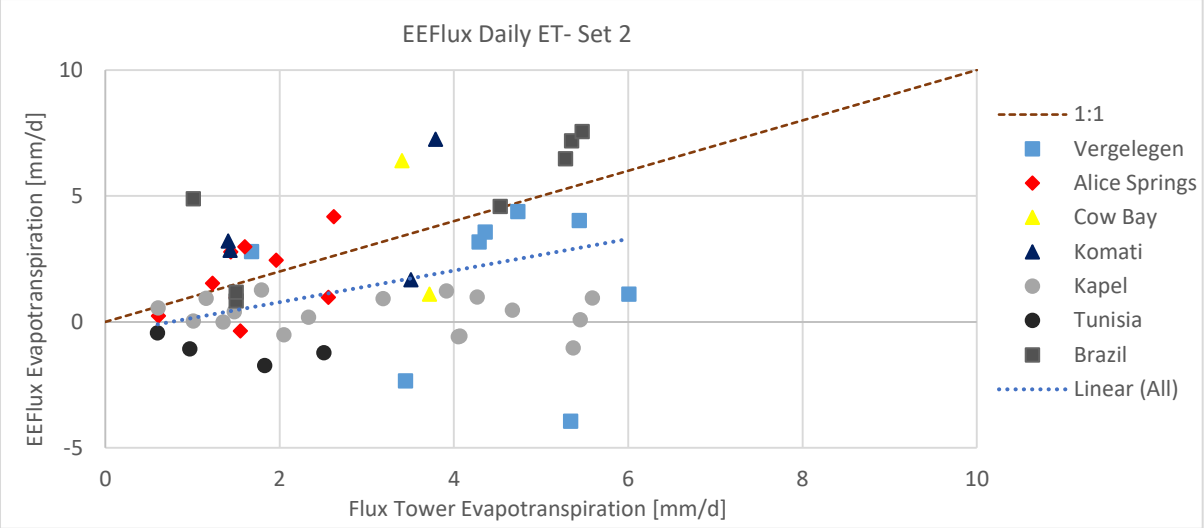

Figure 14: Comparison of daily evapotranspiration rates estimated from EEFlux with flux tower measurements for Set 2 sites.

No changes were made to EEFlux between downloading results for data Set 1 and data Set 2. Even though there were no changes, EEFlux performed better for the second set of flux towers. The RMSE for the second data set was 4.46 mm/d without excluding any outliers. The RMSE values per site for both SEBAL3.0 and EEFlux are listed in Table 5. Results from the second data set for EEFlux did not have the unreasonable values that were higher than 1000 mm/d or smaller than -50 mm/d that the results from Set 1 Netherlands sites had. However, for Set 2, EEFlux estimated negative ET rates, up to -4 mm/d, for a number of overpass days. From all the overpass days, 12 from Tunisia, Kapel, and Vergelegen had negative ET rates. Since other flux components cannot be viewed on the EEFlux interface, an exact explanation for these negative results is not known. ET_rF and reference ET results, which can be viewed in the interface, show negative ET_rF values for these negative ET rate days but positive reference ET values. This indicates that the negative daily ET values did not result from the upscaling to daily values, but that the instantaneous ET values were also negative. Incorrect selection of hot pixels on these days could result in sensible heat values which are overestimated. Overestimation of sensible heat flux values on days with low latent heat flux values could result in negative ET values.

SEBAL3.0 results from Set 2, with changes to the hot and cold pixel constant, did not show the systematic underestimation of daily ET values that appeared in data Set 1 results. The general trend from the second data set is an overestimation of lower ET rates and a slight underestimation of larger ET rates. There is slightly more scatter than Set 1 due to the large overestimation errors for several of the days from the Kapel and Alice Springs sites. Overall, the results are better distributed along the one to one line than prior to the pixel constant adjustment changes, with some overestimates and some underestimates. The RMSE of the SEBAL3.0 daily ET estimates improved slightly from 2.46 mm/d to 2.16 mm/d.

Table 5: RMSE's for both models per site for Set 2 sites.

Site	Number of Overpass days	SEBAL3.0 RMSE [mm/d]	EEFlux RMSE [mm/d]
Vergelegen	9	1.77	8.96
Alice Springs	9	3.24	1.21
Cow Bay	3	1.11	4.12
Komati	4	1.18	2.27
Kapel	17	2.28	3.35
Tunisia	4	0.63	2.82
Brazil	7	1.90	1.88

The instantaneous sensible heat flux results also show changes from the pixel constant adjustment. Figure 15 shows the results of comparison of SEBAL3.0 instantaneous sensible heat flux estimations from Set 2 with flux tower measurements. Similar to daily ET rates, sensible heat flux values are distributed along the one to one line with some overestimations and some underestimations which is an improvement over the systematic overestimation which occurred with Set 1. The sensible heat fluxes from the second data set had an RMSE of 121 W/m^2. This value is largely affected by the results for the Kapel site which had low estimates including 8 days with negative sensible heat fluxes. If this site were removed, the overall RMSE improved to 87 W/m^2.

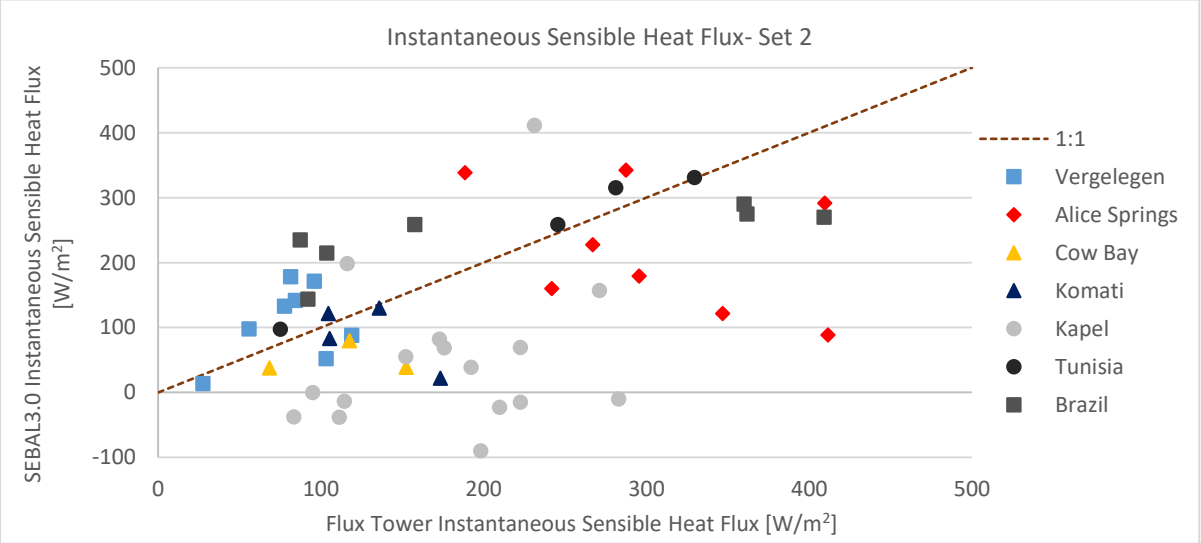

Figure 15: Comparison of SEBAL3.0 sensible heat flux estimations with flux tower measurements for Set 2 sites.

The Kapel site is an irrigated vineyard with very dry landscape surrounding the irrigated area. However, the large errors in the sensible heat flux estimates are the result of incorrect cold pixel selection for this particular area. All of the dates selected for further analysis show cold pixels selected from non-water bodies as well as water bodies. The field is at an elevation of about 65 m and a nearby river has an elevation of 20 m. Both of these areas are near the coast. As you move further inland there is a steep elevation increase and much of the inland area is at a significantly higher elevation than the coast. Cold pixels are being selected along the high elevation side of the demarcation between the high and low elevations. The elevations of the pixels selected from the demarcation range from 600 m to 900 m. The surface temperature map indicates that these areas have much higher temperatures than the water bodies. The cold pixel surface temperatures used to calibrate the sensible heat flux are higher than they should

be due to the inclusion of the surface temperatures along the demarcation. This results in the field with the flux tower having lower surface temperatures than T_{s_cold} values and as a result d*T* values are negative which also results in negative sensible heat fluxes. Cold pixel surface temperatures are still being calculated using the water surface temperatures and are not based on cold vegetation pixels, which are used when the mean water surface temperatures are below 0 °C. The water mask includes areas along the demarcation which is why they are included in the cold pixel selection. Satellite reflectance data is used to calculate the water masks. Since these non-water areas along the demarcation are included in the water mask, the satellite reflectances are the reason for the incorrect classification. NDVI values for these areas are also negative which can indicate the area is water, however, this is false [1]. The Vergelegen site has a similar high/low elevation demarcation, however, at this site the area is not being including in the water mask and the pixel selection appears to be operating as it should.

The Alice Springs site also had incorrect cold pixel selection. There is very little or no water around the Alice Springs flux tower, however, for most images the water mask identified non-water areas as water bodies, which were used for the cold pixel. In several Landsat 7 images the areas identified as water were along the edge of the area with missing data due to the scan line corrector failure. Using these areas as cold pixels resulted in the cold pixel anchor point having higher surface temperatures than they should have. This caused errors in the sensible heat results and daily ET results.

Although Alice Springs and Kapel, where the incorrect cold pixel selection occurred, are both semi-arid regions, the incorrect cold pixel selection was affected by the lack of water and not the climate conditions. Brazil and Tunisia sites had similar climates but these areas had larger water bodies which were selected as cold pixels. Removing the two sites with incorrect cold pixel selection results in an RMSE 0f 1.55 mm/d.

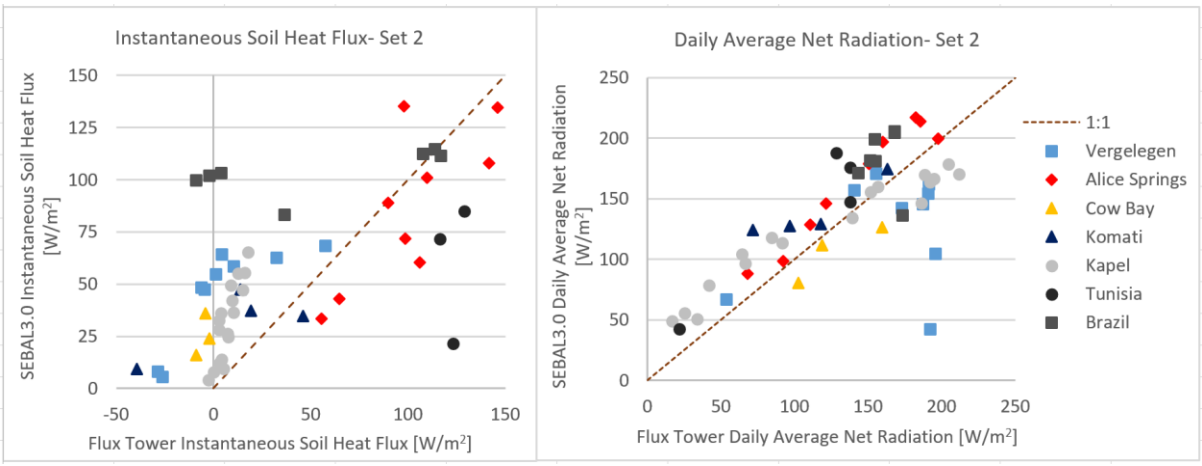

Figure 16: Comparison of SEBAL 3.0 estimates for instantaneous soil heat flux and daily averaged net radiation with flux tower measurements for Set 2 sites.

The instantaneous soil heat flux results in Figure 16 shows very low flux tower measurements with high SEBAL3.0 estimates for the Kapel, Vergelegen, and half of the Brazil overpass days. These two South African site results were for vineyards and the four Brazilian results come from the São Francisco River Basin mango and table grape site. The grapes grown in vineyards and the mangos are both row crops resulting in heterogeneous land. Calculating the soil heat flux of row crops requires extra heat flux plates to take measurements under the plant canopy and between the rows. Multiple plates are required for each area to account for the effect of shade from the crops throughout the day [44]. Since data was

not available on the location and placement of soil heat flux plates for these locations, the measurements could be a source of error. The SEBAL3.0 estimations may also be affected by the row crops. The thermal band on Landsat 5 has a resolution of 120 m, the band on Landsat 7 has a resolution of 60 m, and the thermal bands on Landsat 8 have resolutions of 100 m. These resolutions are too coarse to see the rows and as a result the model may account for more heat flux from the bare soil between rows than the flux tower measurements. Other SEBAL3.0 instantaneous energy flux components comparisons for Set 2 can be found in Appendix D.

As previously mentioned in Section 2.1, SEBAL3.0 uses the evaporative fraction (EF) and daily averaged net radiation to calculate daily ET values. SEBAL3.0 multiplies the instantaneous evaporative fraction by an advection factor to calculate the 24 hr averaged evaporative fraction. This advection factor is calculated in SEBAL3.0 as a function of the 24 hr averaged vapor pressure deficit, which is the 24 hr averaged saturated vapor pressure minus the 24 hr averaged actual vapor pressure, and the instantaneous evaporative fraction. It is uncertain what the exact relationship between these variables and the advection factor is. Figure 17 shows a comparison of the SEBAL3.0 EF_{inst} and EF_{24} compared with flux tower measurement computed values for EF_{inst} and EF_{24}. Some sites had better performance of the EF_{24} than the EF_{inst}. So, in some cases the advection fraction did improve results.

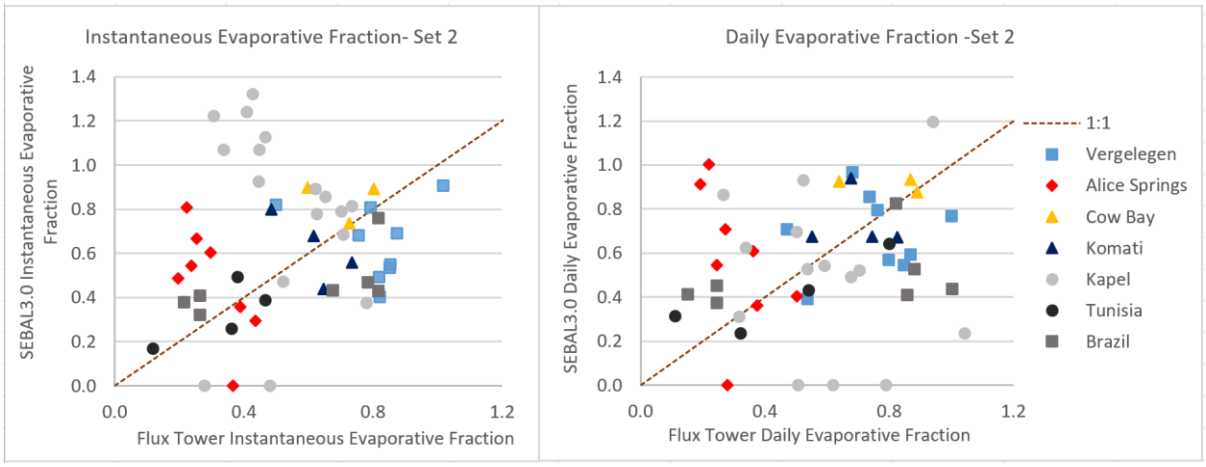

Figure 17: Comparison of SEBAL 3.0 estimates for instantaneous and daily evaporative fraction with instantaneous and daily evaporative fractions calculated from flux tower measurements for Set 2 sites.

To better determine the relationship between the advection fraction and the vapor pressure deficit, and the EF_{inst} and the advection fraction, further analysis was done on the measured values for these variables. Advection factors were calculated for the measured data as the ratio of the EF_{24} to the EF_{inst}. These values were plotted against the corresponding vapor pressure deficit and instantaneous evaporative fraction measured for each day. The plots are located in Appendix E. No substantial relationship was found between either the advection factor and ET_{inst} or the advection factor and the vapor pressure deficit.

Previous applications using SEBAL have assumed that the evaporative fraction remains constant throughout the day when soil moisture does not change and there is no advection [4]. Other research shows EF at overpass time tends to be 10-18% smaller than the daytime average and suggest using a factor of 1.10 or 1.18 to calculate EF_{24} from EF_{inst} to account for advection [45] [46]. In SEBAL3.0 the advection factor is used to account for different advection values depending on the day and region. Figure 18 shows a comparison between the EF values computed from flux tower measurements for

EF_{inst} and $EF_{24.}$ The data from most sites shows a good fit to the one to one line. Days from the Kapel site show the largest deviations. Kapel has the largest average advection factor value of 1.38 calculated from flux tower measurements. The average advection factor for all other Set 2 sites combined was calculated as 1.02. From this value it can be concluded that for the days selected for this study from these sites, there is very little influence from advection, thus the evaporative fraction remains constant throughout the day.

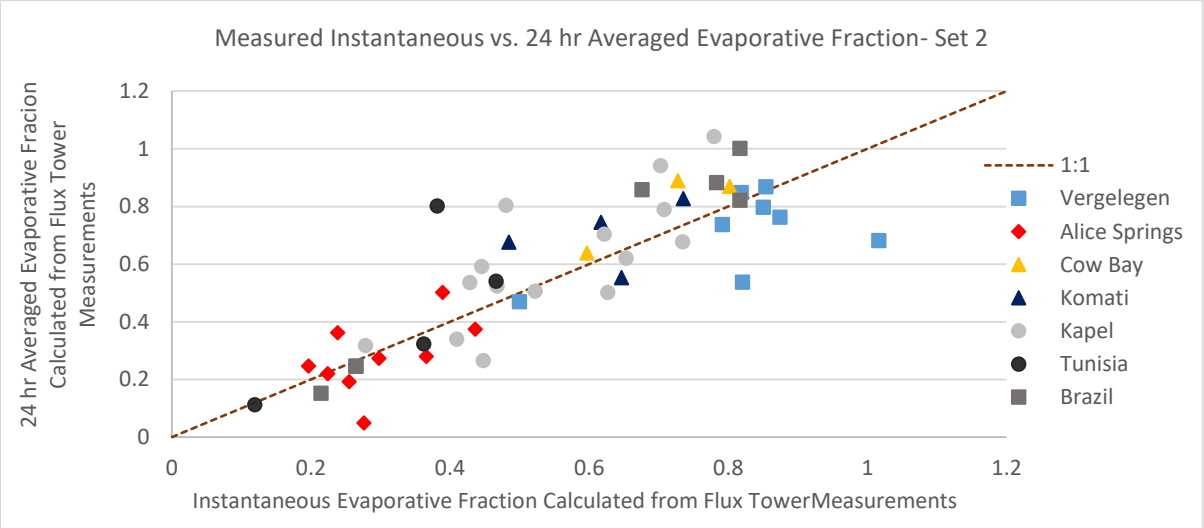

Figure 18: Comparison of instantaneous evaporative fractions with 24 hr averaged evaporative fractions computed from flux tower measurements.

5 Overall Discussion and Recommendations

Daily ET results from both SEBAL3.0 and EEFlux have significantly larger errors than previous studies completed using the non-automated versions SEBAL and METRIC. Average percent errors for daily ET rates for Set 2 sites were calculated as 90% for SEBAL3.0 and 104% for EEFlux. Table 6 shows the average percent error for daily ET rates per site and per model. Averaged errors per site for SEBAL3.0 range from 22% to 218%. The overall error of 90% for SEBAL3.0 is largely affected by the large modelled overestimates of lower ET rates at the Alice Springs and Kapel site. Although Set 1 sites had a systematic underestimation of daily ET rates, there was less scatter than Set 2 rates for SEBAL3.0. The lower amount of scatter resulted in a lower percent error for Set 1 sites. Overall, percent error averages for Set 1 results were 47% for SEBAL3.0 and 118% for EEFlux.

Table 6: Averaged percent error for daily ET rates per site per model for both Set 2 and Set 1.

Set 2 Site	Number of Overpass days	SEBAL3.0 % Error	EEFlux % Error
Vergelegen	9	26	182
Alice Springs	9	218	63
Cow Bay	3	22	89
Komati	4	63	93
Kapel	17	87	81
Tunisia	4	51	182
Brazil	7	78	78
Overall avg.		90	104

Set 1 Site	Number of Overpass days	SEBAL3.0 % Error	EEFlux % Error
Bear River	6	22	45
Palo Verde	15	35	53
Mead	24	46	83
Loobos	11	68	177
Cabauw	7	68	471
Overall avg.		47	118

A previous study of SEBAL stated absolute deviations for individual days were typically 10 to 15% for irrigated crops [47]. A second study found deviations of 1% and a RMSE of 0.38 mm/d for the Brazil sites [43]. A third study evaluating the performance of remote sensing based energy balance models for estimating daily ET in humid subtropical climates in Florida tested both SEBAL and METRIC. In this study, SEBAL estimated daily ET with a RMSE of 0.83 mm/d and METRIC estimated ET with a RMSE of 0.95 mm/d [48]. A fourth study of remote sensing based energy balance models at the Mead, NE site found an average RMSE of 2.07 mm/d for all three Mead flux towers for SEBAL and an average RMSE of 0.86 mm/d for all three Mead flux towers for METRIC [49]. The Mead results from the study discussed in this paper, showed METRIC results with a much higher RMSE of 5.28 mm/d and a RMSE of 2.26 mm/d for SEBAL3.0 before pixel selection constants calibration. All of the performance statistics listed in this section for past research using non-automated model versions come from model runs that have been calibrated and adjusted image by image to achieve optimum results. The automated models in this study require no user interaction other than entering standard meteorological inputs for SEBAL3.0. This lack of user interaction means there is no way for users to influence the results. Comparison of the automated and non-automated performance statistics show better performance for the non-automated versions resulting from the ability to calibrate for each individual scene.

When looking at daily ET results from sites separately there is no clear distinction between sites that perform well and sites that perform poorly. For SEBAL3.0 results, the Tunisia site had the best

performance with a RMSE of 0.63 mm/d. For most other sites there were some days with large deviations from flux tower measurements and some days where SEBAL3.0 estimates were only a few millimetres different than the flux tower measurements. Due to the lack of consistency in site performance, it is not possible to say that the model is able to predict daily ET rates in some climates or areas better than in other climates or areas. RMSE's for the different flux towers at the Brazil location show a lower RMSE for the natural area with a value of 1.65 mm/d than the irrigated area with a value of 2.07 mm/d. The best performing site, Tunisia, also had no irrigation. However, the Komati site with irrigation had an RMSE similar to Cow Bay tropical site and a lower RMSE than the Brazil natural area. From the Set 2 results in this study there was no significant performance difference the accuracy of model performance for irrigated and non-irrigated sites. SEBAL3.0 estimated daily averaged net radiation with the highest accuracy for both Set 1 and Set 2. The estimates for both sites combined, shown in Figure 19, have a good fit with the one to one line and only small amounts scatter. METRIC performed best in Brazil and Alice Springs, however, also had sites where some overpass days had small deviations from measurements and some days at the same site had very large deviations from measurements.

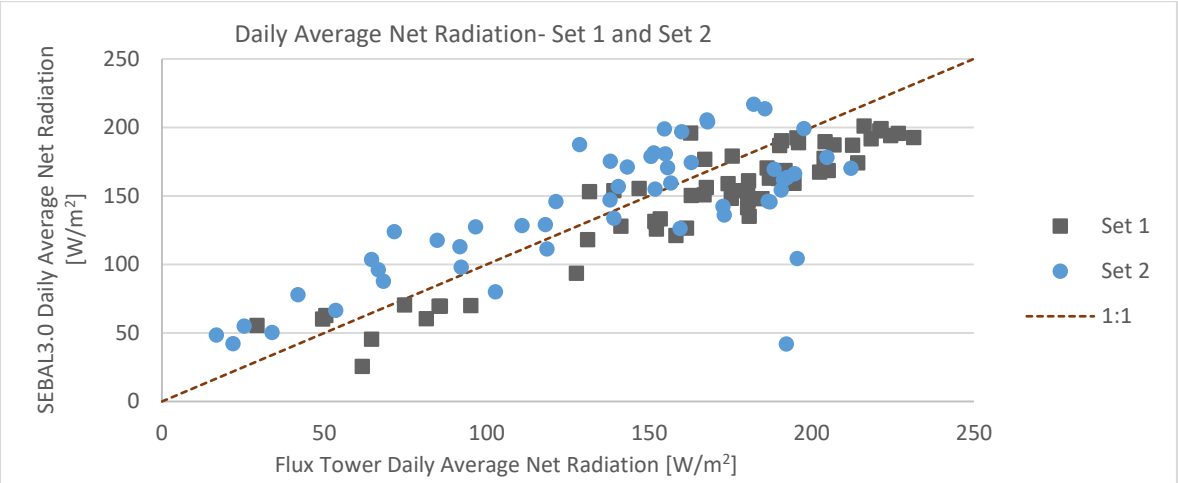

Figure 19: Comparison of daily averaged net radiation for Set 1 and 2 with flux tower measurements.

Generally, remote sensing based ET model results show larger error at the daily time scale and have cumulative estimates that are much closer to flux tower measurements on the monthly or seasonal time scale [47]. However, it was not possible to calculate these cumulative estimates for this study because of the selection of overpass days. Some sites had one selected day per month while others had only several days per year because of the lack of available flux tower measurements and cloud free days. Cumulative values were computed using the sum of all daily ET rates per site. The results can be seen in Table 7. Cumulative errors are much lower than the average for all individual days for all sites, however, still higher than previous non-automated model versions. Eddy covariance data has on average 20% error associated with the measurements [36]. For the eddy covariance sites from Set 2, SEBAL3.0 was able to estimate cumulative daily ET rates within this 20% measurement error for 4 out of 6 eddy covariance sites. The Komati site in Table 7 was excluded from this calculation because the flux tower has a surface renewal system. EEFlux was only able to estimate the cumulative daily ET within the 20% measurement error for 1 out of 6 eddy covariance sites.

Table 7: Cumulative deviations of modeled daily ET estimates from measured daily ET rates.

Set 2 Site	Number of Overpass days	SEBAL3.0 % Error	EEFlux % Error
Vergelegen	9	29	124
Alice Springs	9	132	4
Cow Bay	3	19	50
Komati	4	42	48
Kapel	17	12	90
Tunisia	4	14	176
Brazil	7	13	33

The models both show large deviations from flux tower measurements, however, there is also error associated with the measurements from the different flux tower systems and assumptions made relating to flux tower measurements. Each flux tower system has its own sources of error. For eddy covariance sites, measurement errors can be seen by the lack of closure. In this study latent heat as the residual was the selected choice for closure. Since all the residual from the lack of energy balance closure is classified as latent heat, closure with the residual results in larger latent heat values than closure with the Bowen ratio where the residual is divided between the latent and the sensible heat. The closure method was shown to have an influence on the calibration procedure. The optimum pixel constant combinations were different for direct latent heat measurements, closure as the residual or closure with the Bowen ratio.

Error is also associated with the use of the standard footprint instead of using a footprint model to adjust the footprint size depending on the instrument set up and the conditions on each day. Implications of the standard footprint were discussed in Section 2.5. Both models require standard meteorological inputs which could be another source of error.

A brief analysis of the advection fraction used in SEBAL3.0 was completed and discussed in this report. Advection fractions calculated using measured data showed that for some sites there was an influence from advection throughout the day. Therefore, instantaneous evaporative fractions did not remain constant throughout the day. More analysis can be done on the factors influencing the advection fraction and what their relationship is with the advection factor.

In this study optimum calibration constants for SEBAL3.0 varied per site and per day. However, further research could be completed to see if there is any trend between optimum constant combinations for different climates or land covers. If any optimums for these different conditions were found, the model could be adjusted to allow users to enter calibration constants. Another option would be for the user to develop their own constant combinations for their area of interest if flux tower data were available. For these options, the automated pixel selection procedure would stay the same, but the user could adjust the constants.

This model ran SEBAL3.0 for an area of approximately 100 km^2 from each Landsat scene. The size of the area used can affect the selection of the hot and cold pixels. Hot and cold pixels could be selected from locations quite far away with different conditions than the flux tower location when large areas are used for the model runs. There is also the possibility that parts of an ocean are included in the area which could affect cold pixel selection. In this study the Vergelegen site was very close to the ocean

and a small amount of ocean was included in the area used for SEBAL3.0. The cold pixel group came entirely from the ocean which could possibly have affected results. Further analysis could be done on the size of the area the model should use.

6 Conclusions

Requiring minimum user interaction, SEBAL3.0 and EEFlux are able to produce daily evapotranspiration maps at 30 m resolutions using Landsat satellite data and a surface energy balance. To develop the models, which require no user interaction other than entering some input data, all model processes had to be fully automated. Instead of hot and cold pixels for the self-calibration of the sensible heat flux being selected by the user, the models are now programmed to select these pixels. The automation has increased the number of people who are able to use the models, however, has also resulted in decreases in performance.

SEBAL3.0 produced estimates for daily averaged net radiation with good accuracy. Estimates for the instantaneous evaporative values were not as accurate and showed much more scatter resulting from the scatter in the sensible heat flux estimates. From the calibration of the constants used in selecting hot and cold surface temperature anchor points from the group of hot and cold pixels used in the sensible heat flux calibration, it was concluded that there is no one optimum constant combination that could be used to optimize sensible heat flux estimates. In order to have optimum results, different constants were needed depending on location and time of year. Since SEBAL3.0 had a much lower performance than validations results found in literature for the non-automated model version SEBAL, it was concluded that the automated pixel selection procedure has a large influence on the results of automated models. In order to keep the automated pixel selection, but potentially improve sensible heat flux results, pixel constants could be entered by the user which would allow users to be able to use constants they developed or standardized constants which were developed for different conditions.

EEFlux performance varied per site and produced some results with unreasonable overestimations or underestimations for sites in the Netherlands. EEFlux also produced a large number of negative daily ET rates for several sites. SEBAL did not produce any unreasonable estimations, however, the cold pixel selection did not pick appropriate areas for two sites in very dry semi-arid climates. Overall, SEBAL3.0 had better performance than EEFlux, but EEFlux was able to estimate daily ET rates with lower RMSE's than SEBAL3.0 for two sites, Alice Springs and the Brazil sites. For the second data set, SEBAL3.0 had a RMSE of 2.16 mm/d and EEFlux has a RMSE of 4.46 mm/d. SEBAL3.0 had the best performance for the Tunisia site with a RMSE of 0.63 mm/d. Although both models were able to produce estimates that are very close to flux tower measurements for some days at some sites, the models had inconsistent performance. Both models had a large amount of scatter and very large deviations from flux tower measurements for many days.

Errors, computed using cumulative daily ET values per site, show both models estimate ET rates over a longer time series with more accuracy than on the daily scale. SEBAL3.0 cumulative ET rates had better performance for most sites than EEFlux cumulative rates, with 4 SEBAL3.0 sites having cumulative errors under 20% and only 1 EEFlux site having a cumulative error under 20%. However, neither model was able to produce estimates with the same accuracy as their non-automated versions used in previous studies.

References

[1] R. G. Allen, M. Tasumi, R. Trezza and J. Kjaersgaard, *METRIC Applications Manual for Landsat Satellite Imagery,* Version 2.0.8 ed., Kimberly , Idaho: University of Idaho, 2012.

[2] W. Bastiaanssen, *Regionalization of Surface Flux Densities and Moisture Indicators in Composite Terrain: A Remote Sensing Approach Under Clear Skies in Mediterranean Climates,* Den Haag: CIP Data Koninklijke Bibliotheek, 1995.

[3] R. G. Allen, M. Tasumi and R. Trezza, "Satellite-based energy balance for mapping evapotranspiration with internalized calibration (METRIC)-model," *J. Irrig. Drain. Eng. 133,* pp. 380-394, 2007.

[4] W. Bastiaanssen, E. Noordman, H. Pelgrum, G. Davids, B. Thoreson and R. Allen, "SEBAL Model with Remotely Sensed Data to Improve Water-Resources Management under Actual Field Coonditions," *Journal of Irrigation and Drainage Engineering,* vol. 131, pp. 85-93, 2005.

[5] M. Tasumi, R. Allen and W. Bastiaanssen, "The theoretical basis of SEBAL in Application of the SEBAL methodology for estimating consumptive use of water and streamflow depletion in the Bear River basin of Idaho through remote sensing," Idaho Department of Water Resources and University of Idaho, Department of Biological and Agricultural Engineering, 2000.

[6] D. Long, V. P. Singh and Z.-L. Li, "How sensitive is SEBAL to changes in input variables," *Journal of Geophysical Research,* vol. 116, no. D21107, 2011.

[7] C. Morton, J. Hunntington, G. Pohll, R. Allen, K. McGwire and S. Bassett, "Assessing Calibration Uncertainty and Automation for Estimating Evaportranspiration from Agricultural Areas using METRIC," *Journal of the American Water Resources Association,* vol. 49, no. 3, pp. 549-562, 2013.

[8] A. Kilic, "Using smartphones to track agricultural water use," *Water Current,* vol. 48, no. 1, p. 10, 2016.

[9] W. Bastiaanssen, T. Hessels, P. Trambauer, M. Smiej, Y. Mohamed, J. van Opstal, A. Er-Raji, M. Merdas and K. Biro, *pySEBAL_3.3.1 Code,* UNESCO-IHE, 2016.

[10] H. Rui and H. Beaudoing, "Global Land Data Assimilation System Version 2 (GLDAS-2) Products README," NASA, 2016.

[11] *Landsat—Earth observation satellites (ver. 1.1, August 2016): U.S. Geological Survey Fact Sheet 2015–3081,* U.S. Geological Survey, 2016.

[12] "Shuttle Radar Topography Mission (SRTM) 1 Arc-Second Global," U.S. Geological Survey, January 2015. [Online]. Available: https://lta.cr.usgs.gov/SRTM1Arc.

[13] "GES DISC," NASA Earth Data, March 2012. [Online]. Available: http://disc.sci.gsfc.nasa.gov/hydrology/data-holdings/parameters/sensible_heat_flux.shtml. [Accessed 2016].

[14] "EEFlux," [Online]. Available: http://eeflux-level1.appspot.com/.

[15] A. Kilic, R. Allen, J. Huntington and D. Ozturk, "Google Earth Engine Evapotranspiration Flux-EEFlux," in *2015 International Workshop on Evapotranspiration Mapping for Water Security*, Washington, DC, 2015.

[16] "Land Data Assimilation Systems," NASA, September 2016. [Online]. Available: http://ldas.gsfc.nasa.gov/nldas/.

[17] "University of Idaho Gridded Surface Meteorological Data," [Online]. Available: http://metdata.northwestknowledge.net/. [Accessed 2016].

[18] "Real-Time Mesoscale Analysis (RTMA) Products," Nationnal Centers for Environmental Prediction, January 2014. [Online]. Available: http://www.nco.ncep.noaa.gov/pmb/products/rtma/. [Accessed 2016].

[19] S. e. a. Saha, "NCEP Climate Forecast System Version 2 (CFSv2) 6-hourly Products," Research Data Archive at the National Center for Atmospheric Research, Computational and Information Systems Laboratory, 2011. [Online]. Available: http://rda.ucar.edu/datasets/ds094.0/. [Accessed 2016].

[20] "Soils data for the Conterminous United States Derived from the NRCS State Soil Geographic (STATSGO) Data Base," U.S. Geological Survey, 2000. [Online]. Available: http://water.usgs.gov/GIS/metadata/usgswrd/XML/ussoils.xml. [Accessed 2016].

[21] W. Shangguan, Y. Dai, Q. Duan, B. Lui and H. Yuan, "A global soil data set for earth system modeling," *Journal of Advances in Modeling Earth Systems,* vol. 6, no. 1, pp. 249-263, 2014.

[22] "National Land Cover Database (NLCD)," U.S. Geological Survey, 24 June 2015. [Online]. Available: http://www.mrlc.gov/index.php. [Accessed 2016].

[23] "Land Cover," European Space Agency, 2011. [Online]. Available: http://www.esa-landcover-cci.org/. [Accessed 2016].

[24] Task Committee on Standardization of Reference Evapotranspiration, "The ASCE Standardized Reference Evapotranspiration Equation," American Society of Civil Engineers, Reston, VA, 2005.

[25] R. Allen, B. Burnett, W. Kramber, J. Huntington, J. Kjaersgaard, A. Kilic, C. Kelly and R. Trezza, "Automated Calibration of the Metric-Landsat Evapotranspiration Process," *Journal of the American Water Resources Association,* vol. 49, no. 3, pp. 563-576, 2013.

[26] A. Dong, S. Grattan, J. Carrol and C. Pashar, "Estimation of Daytime Net Radiation over Well-Water Grass," *Journal of Irrigation and Drainage Engineering,* vol. 188, pp. 466--479, 1992.

[27] G. Burba, Eddy Covariance Method for Scientific, Industrial, Agricultural and Regulatory Applications, Lincoln, NE: LI-COR Biosciences, 2013.

[28] T. Foken, Micrometeorology, Springer-Verlag Berlin Heidelberg, 2008.

[29] J. C. van Dam and A. F. Moene, Transport in the Atmoshpere-Vegetation-Soil Continuum, New York: Cambridge University Press, 2014.

[30] J. D. van Opstal, 2013.

[31] I. Bowen, "The ratio of heat losses by conduction and by evaporation," *Physical Review,* vol. 27, pp. 779-787, 1926.

[32] R. W. Todd, S. R. Evett and T. A. Howell, "The Bowen ratio-energy balance method for estimating latent heat flux of irrigated alfalfa evaluated in a semi-arid, advective environment," *Agricultural and Forest Meteorology,* vol. 103, no. 4, pp. 335-348, 2000.

[33] K. Paw U and Y. Brunet, "A surface renewal measure of sensible heat flux density," in *20th Conference on Agricultural and Forest Meteorology,* Salt Lake City, Utah, 1991.

[34] M. Mengistu and M. Savage, "Surface renewal method for estimating sensible heat flux," *Water SA,* vol. 36, pp. 9-18, 2010.

[35] A. H. de C. Teixeira and W. G. M. Bastiaanssen, "Five methods to interpret field measurements of energy fluxes over a micro-sprinkler-irrigated mango orchard," *Irrigation Science,* vol. 30, pp. 13--28, 2012.

[36] K. Wilson, A. Goldstein, E. Falge, M. Aubinet, P. Berbigier, C. Bernhofer, R. Ceulemans, H. Dolman, C. Field, A. Grelle, A. Ibrom, B. Law, A. Kowalski, T. Meyers, J. Moncrieff, R. Monson, W. Oechel, J. Tenhunen, R. Valentini and S. Verma, "Energy Balance Closure at Fluxnet Site," *Agricultural and Forest Meteorology,* vol. 113, pp. 223-243, 2002.

[37] F. Castellví, R. Snyder and D. Baldocchi, "Surface energy-balance closure over rangeland grass using the eddy covariance method and surface renewal analysis," *Agricultural and Forest Meteorology,* vol. 148, no. 6-7, pp. 1147-1160, 2008.

[38] H. Geli, C. Neale and J. Verdin, "Intercomparison of Remote Sensing-Based Models for Evapotranspiration," in *ASA, CSSA, & SSSA International Annual Meeting*, Long Beach, CA, 2014.

[39] "Loobos Site," Climate Exchange, [Online]. Available: http://www.climatexchange.nl/sites/loobos/. [Accessed 2016].

[40] "Cabauw Experimental site for Atmospheric Research," 8 August 2016. [Online]. Available: http://www.cesar-observatory.nl/. [Accessed 2016].

[41] "Monitoring Sites - Alice Springs," Oz Flux, 2016. [Online]. Available: http://www.ozflux.org.au/monitoringsites/alicesprings/alicesprings_description.html. [Accessed 2016].

[42] "Monitoring Sites - Cow Bay," Oz Flux, 2016. [Online]. Available: http://www.ozflux.org.au/monitoringsites/cowbay/cowbay_description.html. [Accessed 2016].

[43] A. d. C. Teixeira, W. Bastiaanssen, M. Ahmad and M. Bos, "Reviewing SEBAL input parameters for assessing evapotranspiration and water productivity for the Low-Middle Sao Francisco River basin, Brazil: Part A: Calibration and validation," *Agricultural and Forest Meteorology,* vol. 149, pp. 462-476, 2009.

[44] C. Poblete-Echeverría and S. Ortega-Farias, "Estimation of Vineyard Evapotranspiration using the Surface Renewal and Residual Energy Balance Methods," *Acta horticulturae*, pp. 633-638, 2014.

[45] A. Teixeira, W. Bastiaanssen, M. Moura, J. Soares, M. Ahmad and M. Bos, "Energy and water balance measurements for water productivity analysis in irrigated mango trees, Northeast Brazil," *Agricultural and Forest Meteorology,* vol. 148, pp. 1524-1537, 2008.

[46] M. Anderson, J. Norman, G. Diak, W. Kustas and J. Mecikalski, "A two-source time-integrated model for estimating surface fluxes using thermal infrared remote sensing," *Remote Sensing of Environment,* vol. 60, pp. 195-216, 1997.

[47] W. Bastiaanssen, I. Miltenburg, R. Evans, R. Molloy, F. Bastiaanssen and E. van derr Pol, "An operational satellite-based irrigation monitoring and scheduling tool for saving water in irrigation," in *Irrigation and Drainage Conference*, Swan Hill, Australia, 2009.

[48] N. Bhattarai, S. Shaw, L. Quackenbush and J. Im, "Evaluating five remote sensing based single-source surface energy balance models for estimating daily evapotranspiration in a humid subtropical climate," *International Journal of Allpied Earth Observation and Geoinformation,* vol. 49, pp. 75-86, 2016.

[49] R. Singh and G. Senay, "Comparison of Four Different Energy Balancce Models for Estimating Evapotranspiration in the Midwestern United States," *Water*, 2015.

[50] "Landsat Missions," U.S. Geological Survey, 30 May 2013. [Online]. Available: http://landsat.usgs.gov/naming_conventions_scene_identifiers.php. [Accessed 2016].

[51] "GlobCover," European Space Agency, [Online]. Available: http://due.esrin.esa.int/page_globcover.php. [Accessed 2016].

Appendix A: Sensible Heat Flux Iteration

The iterative procedure needed to solve for H and r_{ah} is shown in Figure 20. The aerodynamic resistance to heat transport is needed to solve for sensible heat flux and sensible heat flux is needed to make a correction to r_{ah} to account for the effects of buoyancy of heated, light air at the surface [1].

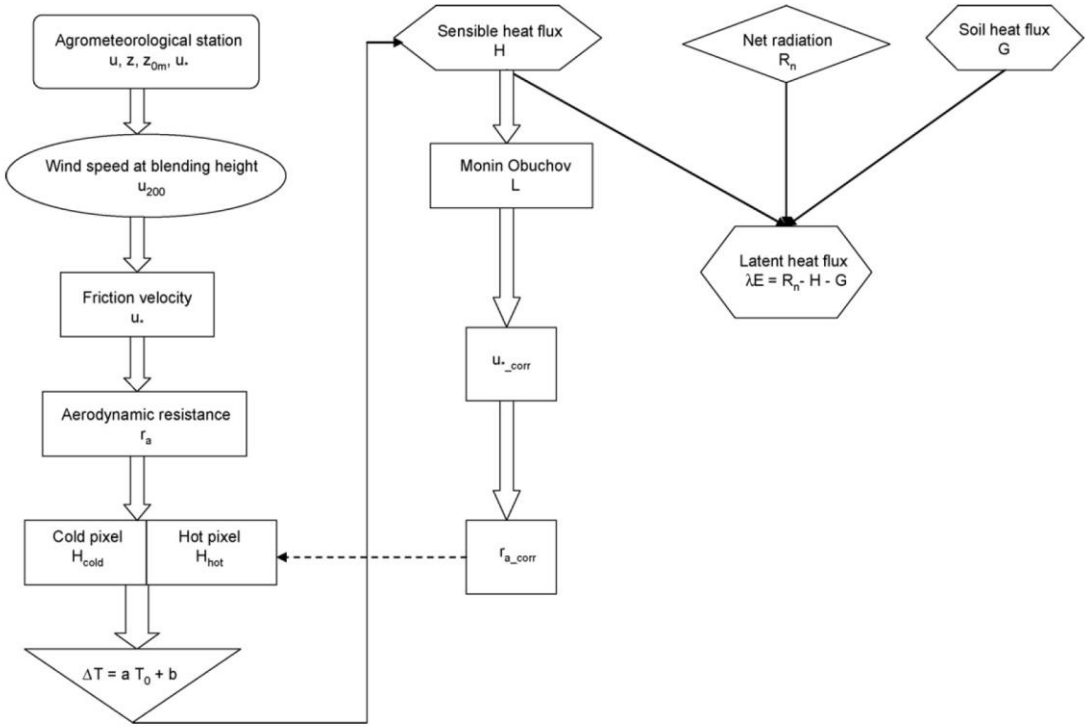

Figure 20: Flowchart for the sensible heat flux calibration including the iterative procedure needed to solve for the sensible and aerodynamic resistance to heat transport [43].

Figure 21 shows the iterative procedure used in the automated pixel selection procedure developed for METRIC which was discussed in Section 2.2.

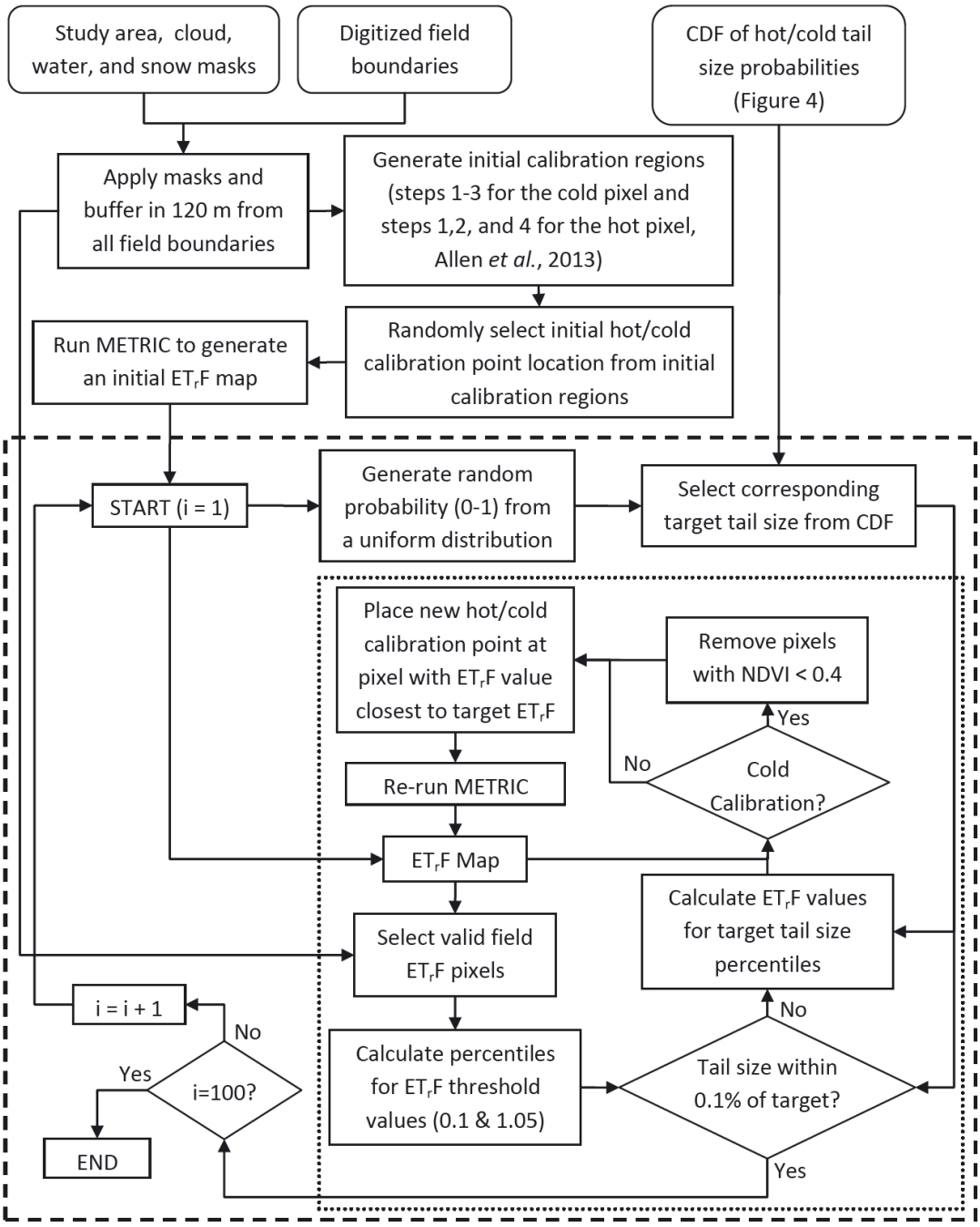

Figure 21: Flowchart for automated pixel selection procedure developed for METRIC by Morton et al. [7]. Dashed box shows the Monte Carlo process and dotted box is the iterative process to select hot and cold pixels based on target tail sizes in the ET_rF distribution.

Appendix B: Set 1 Sites Results and Inputs

Figure 22 and Figure 23 show Set 1 SEBAL3.0 results for instantaneous energy balance components.

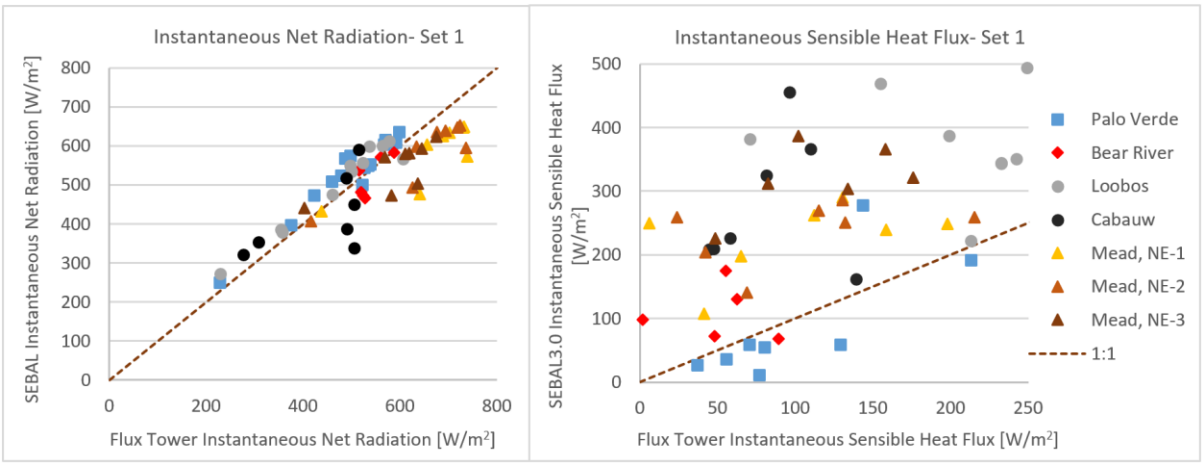

Figure 22: Comparison of SEBAL3.0 instantaneous net radiation and instantaneous sensible heat flux results with flux tower measurements for Set 1 sites.

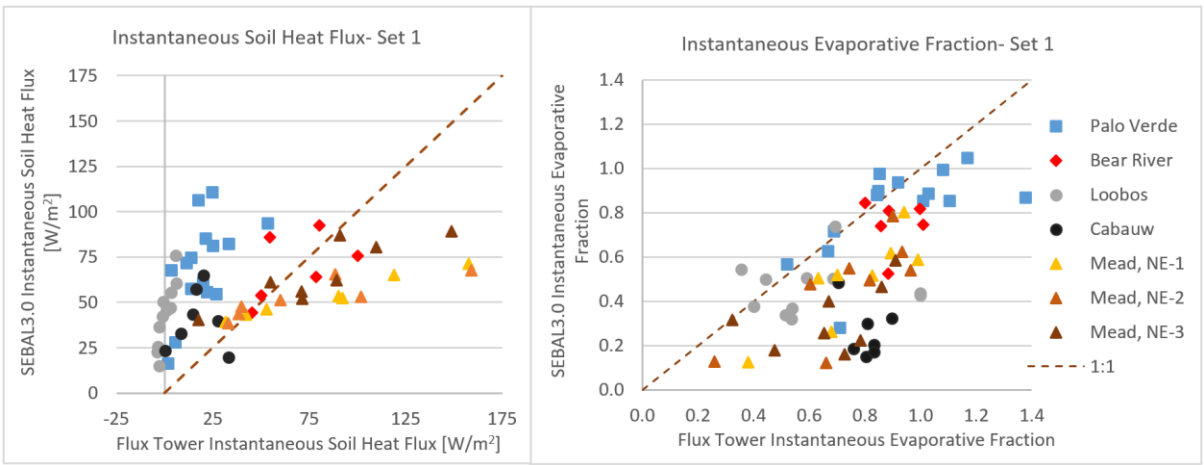

Figure 23: Comparison of SEBAL3.0 instantaneous soil heat flux and instantaneous evaporative fraction results with flux tower measurements for Set 1 sites.

Table 8 lists all the meteorological data that was used as inputs for the SEBAL3.0 model.

Landsat scenes listed on the input tables have the following naming convention [50].

LXSPPPRRRYYYYDDDGSIVV
L = Landsat
X = Sensor
S = Satellite
PPP = WRS path
RRR = WRS row
YYYY = Year
DDD = Julian day of year
GSI = Ground station identifier
VV = Archive version number

Table 8: Input meteorological data for Set 1 Sites.

Name	Landsat scene	Year	DOY	Mth	Day	Temp_Inst [C]	Temp_24 [C]	RH_inst [%]	RH_24 [%]	zx	Wind_inst [m/s]	Wind_24 [m/s]	Rs_24 W/m^2	Rs_in_inst W/m^2	Wind degrees	Wind Dir.
Bear River	LC80390312013183LGN00	2013	183	7	2	31.3	28.1	27.5	30.3	3	1.7	3.4	329.1	915.3	18	N
""	LC80390312013199LGN00	2013	199	7	18	31.1	26.1	35.6	41.3	3	0.9	2.7	306.3	880.2	342	N
""	LC80390312013215LGN00	2013	215	8	3	27.4	22.6	22.6	26.6	3	2.6	3.4	310.8	886.9	184	S
""	LC80380312013240LGN01	2013	240	8	28	27.1	22.6	40.7	56.2	3	3.5	1.8	273.1	798.2	178	S
""	LC80390312013247LGN00	2013	247	9	4	26.1	22.2	50.3	67.1	3	1.3	1.4	257.6	774.8	166	S
Loobos	LE71980242013121EDC00	2013	121	5	1	15.4	10.5	46.0	61.8	1.5	5.0	4.6	276.0	788.9	83	E
""	LC81970242013202LGN00	2013	202	7	21	28.7	23.2	37.0	58.3	1.5	4.0	2.7	312.6	808.3	110	E
""	LE71980242013217ASN00	2013	217	8	5	27.6	22.8	40.0	61.5	1.5	4.0	2.8	247.7	766.7	186	S
""	LC81980242013273LGN00	2013	273	9	30	13.8	10.4	51.0	61.0	1.5	6.0	4.8	157.2	544.4	91	E
""	LE71970242013274ASN00	2013	274	10	1	14.2	9.6	59.0	71.8	1.5	5.0	4.3	158.3	533.3	86	E
""	LE71980242013297ASN00	2013	297	10	24	14.7	11.2	66.0	84.4	1.5	4.0	2.7	96.5	391.7	218	S
""	LE71970242012144ASN00	2012	144	5	23	28.2	20.4	51.0	77.0	1.5	2.0	1.9	219.3	780.6	273	W
""	LE71980242012231ASN00	2012	231	8	18	28.9	25.2	45.0	60.2	1.5	5.0	3.0	250.5	683.3	156	S
""	LE71980242011100ASN00	2011	100	4	10	15.2	10.7	42.0	66.9	1.5	2.0	1.9	221.6	652.8	60	E
""	LT51980242011108MOR00	2011	108	4	18	17.7	13.6	33.0	51.0	1.5	6.0	3.5	254.2	730.6	126	E
""	LE71980242011116ASN00	2011	116	4	26	20.8	15.1	33.0	51.8	1.5	6.0	4.7	244.2	733.3	57	E
Cabauw	LC81980242014068LGN00	2014	68	3	9	15.1	11.3	49.0	62.5	1.5	5.0	3.6	158.0	519.4	180	S
""	LE71980242014204ASN00	2014	204	7	23	26.7	23.2	48.0	62.1	1.5	6.0	4.3	310.8	802.8	56	E
""	LC81980242014212LGN00	2014	212	7	31	22.6	18.8	60.0	77.5	1.5	4.0	2.2	254.1	772.2	183	S
""	LC81980242014276LGN00	2014	276	10	3	20.3	15.0	72.0	87.5	1.5	2.0	1.5	145.3	508.3	121	E
""	LE71980242013121EDC00	2013	121	5	1	14.5	10.5	45.0	59.7	1.5	5.0	4.0	276.7	777.8	52	E
""	LE71980242013217ASN00	2013	217	8	5	27.1	21.8	50.0	70.2	1.5	4.0	2.7	252.0	769.4	198	S
""	LC81980242013273LGN00	2013	273	9	30	15.9	10.4	57.0	64.6	1.5	7.0	4.7	163.2	561.1	83	E

Table 8 continued…

Name	Landsat scene	Year	DOY	Mth	Day	Temp_Inst	Temp_24	RH_inst	RH_24	zx	Wind_inst	Wind_24	Rs_24	Rs_in_inst	Wind	Wind
						[C]	[C]	[%]	[%]		[m/s]	[m/s]	W/m^2	W/m^2	degrees	Dir.
Palo Verde	LT50380372008019EDC00	2008	19	1	19	11.7	7.2	35.0	46.0	2	3.5	1.8	146.0	427.0	358	N
""	LT50380372008067PAC01	2008	67	3	7	18.4	13.6	17.0	29.0	2	3.7	1.9	219.0	629.0	339	N
""	LT50380372008083PAC01	2008	83	3	23	22.5	18.3	21.0	30.0	2	3.1	2.2	262.0	725.0	357	N
""	LT50380372008099PAC01	2008	99	4	8	21.9	18.4	34.0	40.0	2	2.1	3.3	270.0	775.0	171	S
""	LT50380372008115PAC01	2008	115	4	24	22.8	18.3	32.0	43.0	2	4.4	2.4	305.0	830.0	313	W
""	LT50380372008131PAC01	2008	131	5	10	27.5	23.4	28.0	36.0	2	1.6	1.4	301.0	801.0	44	N
""	LT50380372008147PAC01	2008	147	5	26	20.9	18.8	43.0	51.0	2	1.5	1.9	325.0	838.0	17	N
""	LT50380372008163PAC02	2008	163	6	11	34.0	28.3	8.0	25.0	2	3.8	2.1	337.0	859.0	338	N
""	LT50380372008195PAC01	2008	195	7	13	33.5	31.2	47.0	55.0	2	2.0	2.3	301.0	753.0	186	S
""	LT50380372008211PAC01	2008	211	7	29	32.3	29.3	35.0	42.0	2	3.6	2.5	300.0	762.0	171	S
""	LT50380372008259PAC01	2008	259	9	15	32.5	27.8	42.0	46.0	2	1.8	1.6	246.0	699.0	332	N
""	LE70380372008139EDC00	2008	139	5	18	33.1	28.6	32.0	39.0	2	0.8	1.3	313.0	815.0	136	S
""	LE70380372008155EDC00	2008	155	6	3	29.4	25.0	32.0	40.0	2	1.1	2.1	322.0	809.0	334	N
""	LE70380372008171EDC00	2008	171	6	19	35.1	30.8	43.0	46.0	2	1.2	1.3	336.0	835.0	120	E
""	LE70380372008235EDC00	2008	235	8	22	32.5	29.4	44.0	45.0	2	2.6	2.4	285.0	761.0	181	S
Mead	LE70280312012112EDC00	2012	112	4	21	17.3	13.2	41.2	51.0	3	5.62	4.73	224.5	752.0		W
" "	LE70280312012128EDC00	2012	128	5	7	17.4	14.7	54.5	61.9	3	5.80	4.20	235.2	791.0		N
" "	LE70280312012160EDC00	2012	160	6	8	28.5	24.9	40.6	45.8	3	5.35	4.11	330.3	896.0		S
" "	LE70280312012176EDC00	2012	176	6	24	29.6	26.9	67.5	77.4	3	2.27	2.47	314.6	887.0		E
" "	LE70280312012192EDC00	2012	192	7	10	27.5	22.6	40.1	65.2	3	3.04	1.71	329.4	899.0		E
" "	LE70280312012208EDC00	2012	208	7	26	32.0	27.7	45.0	64.4	3	2.19	1.99	310.3	854.0		N
" "	LE70280312012240EDC00	2012	240	8	27	29.7	23.8	52.5	69.8	3	2.13	1.35	258.7	791.0		S
" "	LE70280312012288EDC00	2012	288	10	14	16.2	13.2	43.5	63.8	3	7.39	4.40	196.4	716.0		N

Appendix C: Data Set 1 Pixel Selection Constant Calibration Additional Results

Figures 24, 25, 26, and 27 show the calibration procedure results for the Palo Verde and Loobos site. The calibration procedure results for the Mead site were shown in Section 4.2.

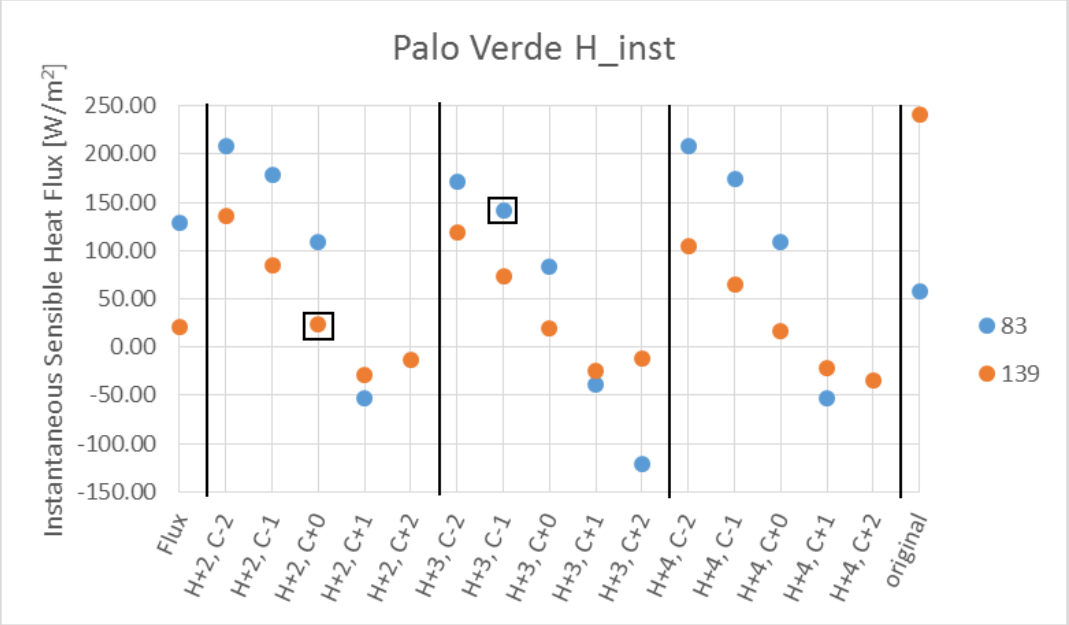

Figure 24: Instantaneous sensible heat flux values for all 15 pixel constant combinations for days 83 and 139 at Palo Verde. Flux tower sensible heat measurements are shown on the left side and original SEBAL3.0 estimates before calibration procedure are shown on the right side. Boxes indicate the best pixel combination per site per day.

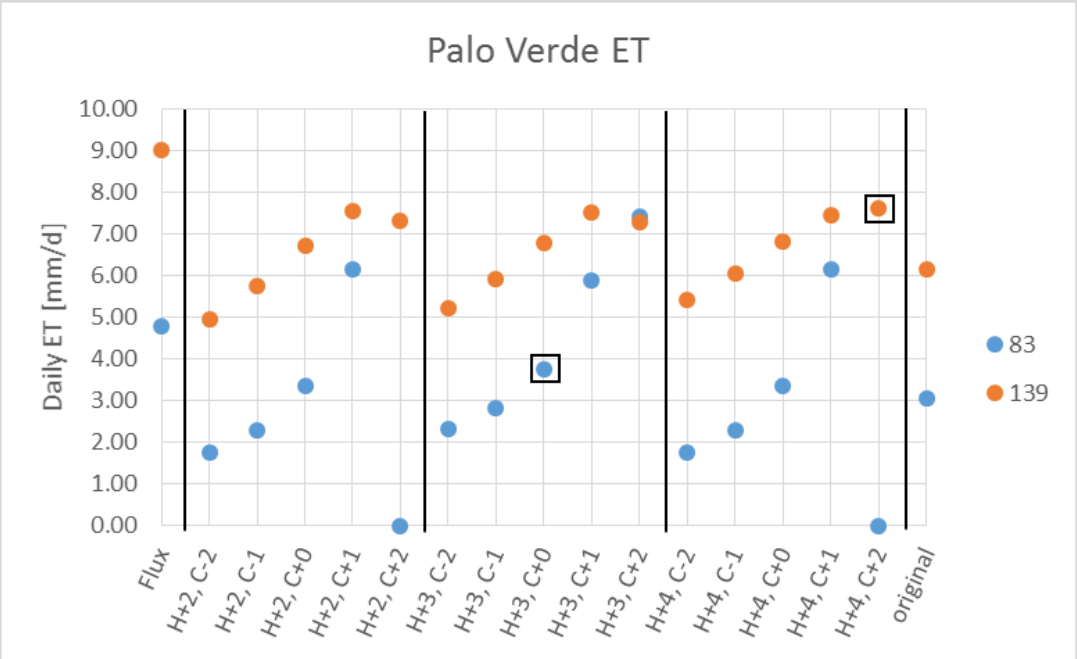

Figure 25: Daily evapotranspiration values for all 15 pixel constant combinations for days 83 and 139 at Palo Verde. Daily ET values calculated from latent heat values from the Bowen ratio flux tower are shown on the left side. Results from original pixel constants before calibration shown on the right side. Boxes indicate the best pixel combination per site per day based on the closest combination to the measurement data closed using the latent heat as residual.

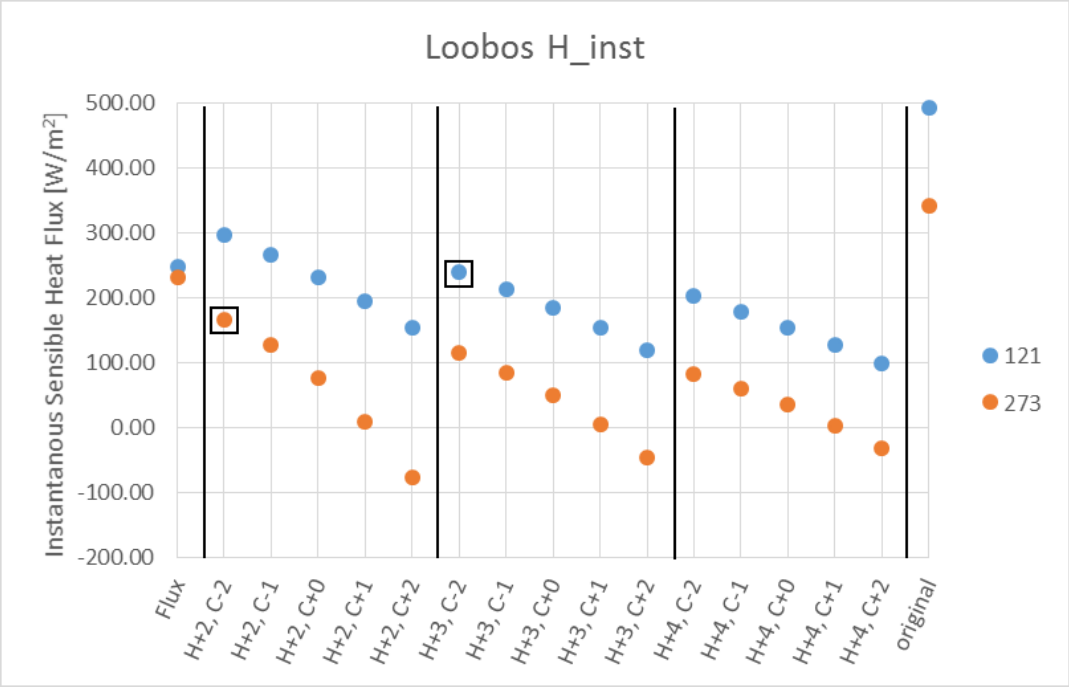

Figure 26: Instantaneous sensible heat flux values for all 15 pixel constant combinations for days 121 and 273 at Loobos. Flux tower sensible heat measurements are shown on the left side and original SEBAL3.0 estimates before calibration procedure are shown on the right side. Boxes indicate the best pixel combination per site per day.

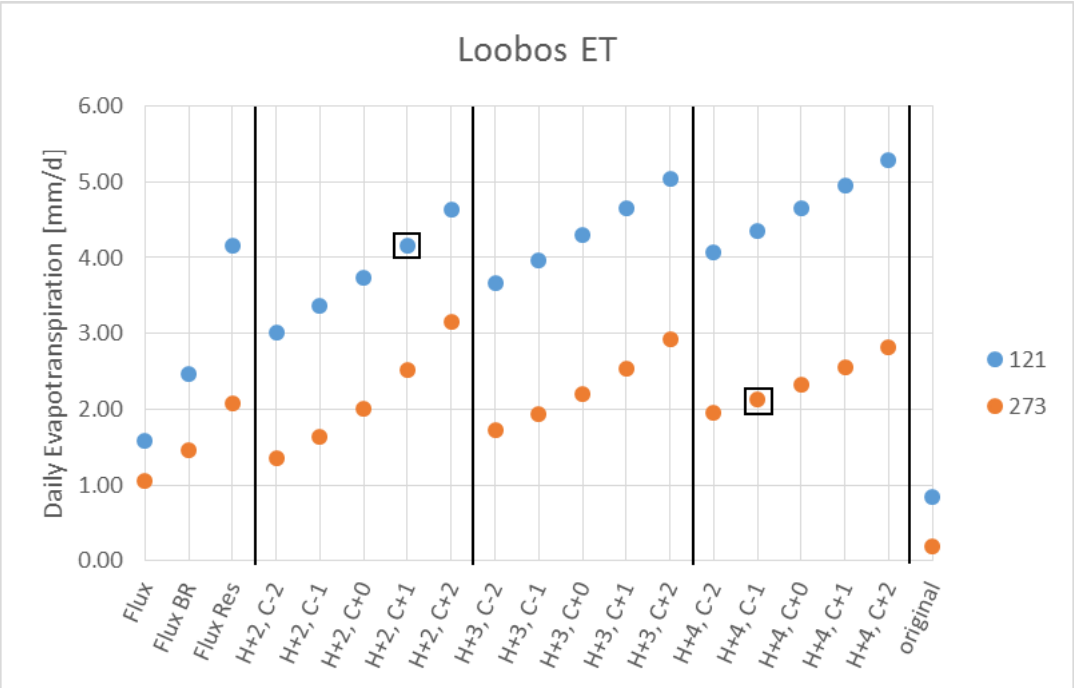

Figure 27: Daily evapotranspiration values for all 15 pixel constant combinations for days 121 and 273 at Loobos. Directly measured and adjusted for closure flux tower measurements are shown on the left side. "Flux" is the daily ET calculated from direct λE measurements. "Flux BR" is daily ET calculated from λE measurements closed with the Bowen Ratio and "Flux Res" is daily ET calculated from λE measurements closed using λE as the residual. Results from original pixel constants before calibration shown on the right side. Boxes indicate the best pixel combination per site per day based on the closest combination to the "Flux Res" measurement data which is closed using the latent heat as the residual.

Appendix D: Set 2 Sites Results and Inputs

Figure 28 and Figure 29 show SEBAL3.0 results for instantaneous energy balance components from Set 2.

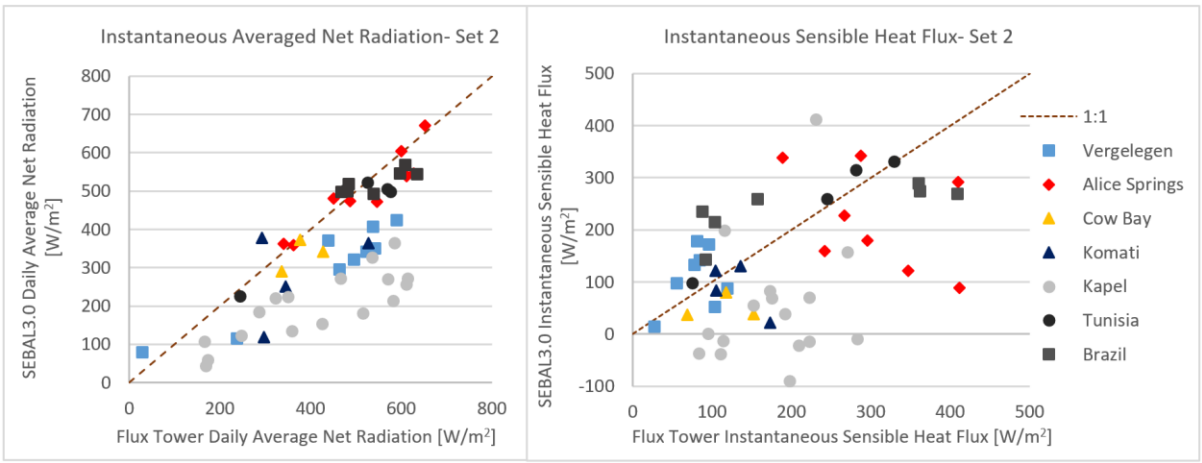

Figure 28: Comparison of SEBAL3.0 instantaneous net radiation and instantaneous sensible heat flux results with flux tower measurements for Set 2 sites.

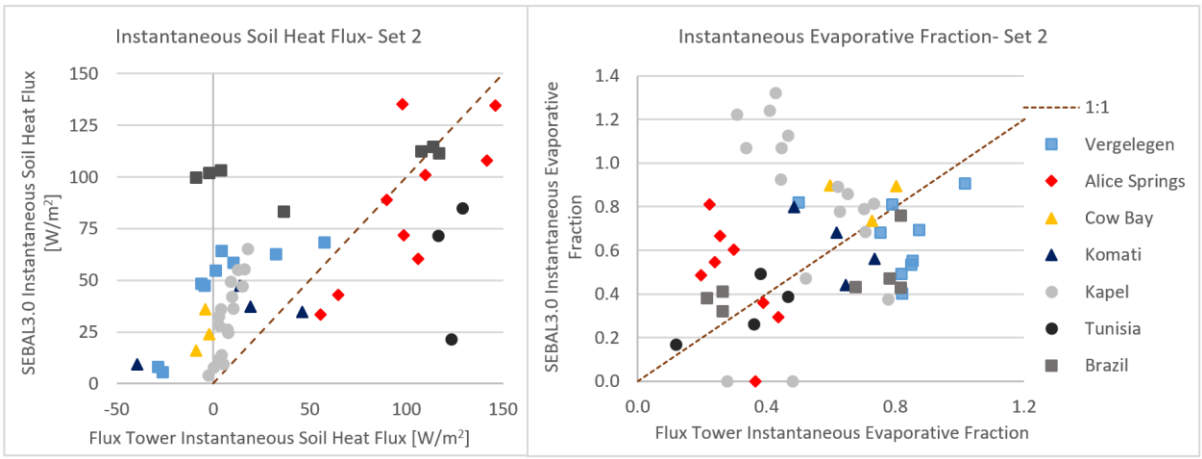

Figure 29: Comparison of SEBAL3.0 instantaneous soil heat flux and instantaneous evaporative fraction results with flux tower measurements for Set 2 sites.

Table 9 lists all the meteorological data that was used as inputs for the SEBAL3.0 model.

Table 9: Input meteorological data for Set 2 sites

Name	Landsat scene	Year	DOY	Mth	Day	Temp_Inst	Temp_24	RH_inst	RH_24	zx	Wind_inst	Wind_24	Rs_24	Rs_in_inst	Wind	Wind
						[C]	[C]	[%]	[%]		[m/s]	[m/s]	W/m^2	W/m^2	degrees	Dir.
Vergelegen	LC81750842015006LGN00	2015	6	1	6	21.1	22.9	72.8	61.9	3	0.2	0.2	257.6	673.2	296	W
""	LE71750842015014JSA00	2015	14	1	14	26.1	27.4	53.1	48.7	3	0.2	0.2	242.2	620.7	303	W
""	LC81750842015022LGN00	2015	22	1	22	32.4	26.6	30.2	49.2	3	0.3	1.0	229.2	572.6	299	W
""	LC81750842015038LGN00	2015	38	2	7	27.8	23.3	40.7	54.3	3	0.2	0.2	222.4	542.7	290	W
""	LC81750842015054LGN00	2015	54	2	23	25.3	23.7	33.6	41.1	3	0.2	1.0	279.2	515.1	321	N
""	LE71750842015062JSA00	2015	62	3	3	34.9	32.9	15.4	20.3	3	0.2	0.8	265.5	483.2	287	W
""	LE71750842015158SG100	2015	158	6	7	12.2	14.2	59.0	52.0	3	0.2	0.2	112.1	161.1	299	W
""	LE71750842015222ASN00	2015	222	8	10	10.1	11.5	50.2	50.2	3	0.2	0.2	156.5	223.3	315	N
""	LE71750842015334SG100	2015	334	11	30	25.2	26.7	51.5	41.7	3	0.2	0.2	162.6	663.0	306	W
Kapel	LC81750822014243LGN00	2014	243	8	31	20.3	23.4	26.2	21.6	3	4.8	3.7	197.0	351.4	79	E
""	LE71750822014299SG100	2014	299	10	26	27.2	29.7	32.5	28.3	3	6.6	5.3	264.2	518.0	84	E
""	LC81750822014323LGN00	2014	323	11	19	28.3	26.1	28.6	38.2	3	1.2	2.1	281.5	536.9	326	N
""	LC81750822014355LGN00	2014	355	12	21	21.5	20.4	44.6	51.3	3	3.2	2.7	294.8	525.6	194	S
""	LC81750822015006LGN00	2015	6	1	6	25.6	26.1	57.5	56.5	3	2.3	1.9	272.7	465.7	108	E
""	LE71750822015046ASN00	2015	46	2	15	23.6	24.0	33.1	38.9	3	4.8	3.1	266.3	426.0	113	E
""	LC81750822015070LGN00	2015	70	3	11	19.6	21.7	64.2	58.3	3	1.2	1.3	227.8	351.0	322	N
""	LE71750822015094ASN00	2015	94	4	4	13.1	17.8	85.5	63.6	3	1.9	2.4	196.3	266.5	302	W
""	LE71750822015126JSA00	2015	126	5	6	16.4	18.6	51.8	45.7	3	2.2	2.6	159.3	231.3	132	E
""	LC81750822015182LGN00	2015	182	7	1	10.9	16.0	84.0	55.7	3	0.4	1.9	122.6	147.8	136	S
""	LC81750822015262LGN00	2015	262	9	19	18.5	22.0	30.2	27.7	3	7.8	6.7	210.5	434.7	108	E
""	LE71750822015334SG100	2015	334	11	30	32.0	27.6	19.0	33.6	3	0.8	1.5	273.3	581.8	359	N
""	LC81750822016009LGN00	2016	9	1	9	29.6	27.4	30.8	37.9	3	1.9	2.4	268.1	531.1	315	N
""	LC81750822016041LGN00	2016	41	2	10	22.6	23.9	68.1	64.2	3	0.9	1.9	228.3	405.7	323	N
""	LE71750822016097ASN00	2016	97	4	6	23.2	25.1	34.4	27.5	3	3.7	4.0	174.7	353.6	101	E
""	LC81750822016153LGN00	2016	153	6	1	13.8	16.0	63.5	61.0	3	0.7	1.1	107.2	205.0	82	E
""	LC81750822016185LGN00	2016	185	7	3	14.7	17.1	29.1	25.8	3	3.1	4.9	109.2	199.4	121	E

Table 9 Continued…

Name	Landsat scene	Year	DOY	Mth	Day	Temp_Inst	Temp_24	RH_inst	RH_24	zx	Wind_inst	Wind_24	Rs_24	Rs_in_inst	Wind	Wind
						[C]	[C]	[%]	[%]		[m/s]	[m/s]	W/m^2	W/m^2	degrees	Dir.
Komati	LE71680782012101ASN00	2012	101	4	10	19.1	20.7	76.3	62.0	10	0.9	2.8	238.4	210.9	102	E
""	LE71680782012213ASN00	2012	213	7	31	15.9	16.8	80.8	66.0	10	1.9	2.7	175.9	76.8	84	E
""	LE71680782012245ASN00	2012	245	9	1	24.0	22.6	32.1	52.0	10	3.6	5.7	211.8	399.0	223	S
""	LE71680782012277ASN00	2012	277	10	3	23.5	23.3	53.2	59.0	10	2.7	3.1	270.8	530.6	92	E
Cow Bay	LC80960712015029LGN00	2015	29	1	29	31.2	29.5	46.5	49.0	45	1.3	2.1	191.9	506.5	349	N
""	LE70960712015117ASA00	2015	117	4	27	25.2	24.4	52.0	56.7	45	2.4	2.1	119.7	374.3	36	N
""	LE70960712015261ASA00	2015	261	9	18	23.7	22.0	68.0	67.8	45	2.1	2.2	164.0	488.1	41	N
Ti Tree	LC81030752014011LGN00	2014	11	1	11	34.9	32.0	16.7	13.0	9.8	4.6	3.07	354.9	888.5	100	E
""	LE71030752014051ASA00	2014	51	2	20	25.1	25.4	26.7	25.0	9.8	4.7	3.64	354.8	854.5	133	E
""	LC81030752014075LGN00	2014	75	3	16	31.6	30.9	27.4	28.6	9.8	4.2	2.49	296.5	769.1	303	W
""	LC81030752014107LGN00	2014	107	4	17	23.6	21.6	25.6	30.4	9.8	4.7	2.60	269.0	714.9	116	E
""	LE71030752014115ASA00	2014	115	4	25	25.8	23.3	24.0	24.9	9.8	4.1	2.1	248.0	670.8	108	E
""	LE71030752014179ASA00	2014	179	6	28	13.3	12.7	32.4	30.7	9.8	4.7	3.0	206.8	551.1	162	S
""	LC81030752014203LGN00	2014	203	7	22	19.3	17.7	22.5	30.9	9.8	2.6	2.0	208.5	547.9	44	N
""	LC81030752013312LGN00	2013	312	11	8	31.1	30.7	17.3	15.1	9.8	5.5	3.4	332.9	915.4	105	E
""	LE71030752013336ASA00	2013	336	12	2	33.4	31.8	33.3	35.6	9.8	2.9	2.4	304.8	905.4	3	N
Tunisia	LE71910352012022ASN00	2012	22	1	22	16.2	11.6	54.0	70.2	2.3	3.6	1.6	130.0	525.2		W
""	LE71910352012118EDC00	2012	118	4	27	24.9	20.4	36.4	49.6	2.3	2.5	2.0	344.7	974.0		E
""	LE71910352012134ASN00	2012	134	5	13	29.8	25.3	22.2	47.2	2.3	2.8	2.5	368.5	964.0		W
""	LE71910352012150ASN00	2012	150	5	29	26.3	27.8	48.9	53.1	2.3	2.5	2.0	257.3	972.0		N

Table 9 continued…

Name	Landsat scene	Year	DOY	Mth	Day	Temp_Inst	Temp_24	RH_inst	RH_24	zx	Wind_inst	Wind_24	Rs_24	Rs_in_inst	Wind	Wind
						[C]	[C]	[%]	[%]		[m/s]	[m/s]	W/m^2	W/m^2	degrees	Dir.
Brazil	LT52170662003267CUB00	2003	267	9	24	26.5	25.8	55.8	48.0	3	5.5	2.4	256.9	833.6		E
""	LT52170662004286CUB00	2004	286	10	12	27.8	28.1	52.1	46.0	3	6.2	3.4	309.0	856.5		E
""	LT52170662004318CUB00	2004	318	11	13	31.8	31.4	50.7	39.0	3	4.8	2.5	324.1	844.6		E
""	LT52170662005288CUB00	2005	288	10	15	28.2	28.1	50.6	45.0	3	5.3	3.0	317.1	858.0		E
""	LT52170662005320CUB00	2005	320	11	16	29.9	28.2	50.9	48.0	3	4.3	2.6	324.1	863.7		E

Appendix E: Advection Factor Plots

Figure 30 shows the relationship between the advection factors calculated from flux tower measurements and the 24 hr averaged vapor pressure deficit. Figure 31 shows the relationship between the advection factors calculated from flux tower measurements and instantaneous evaporative fractions.

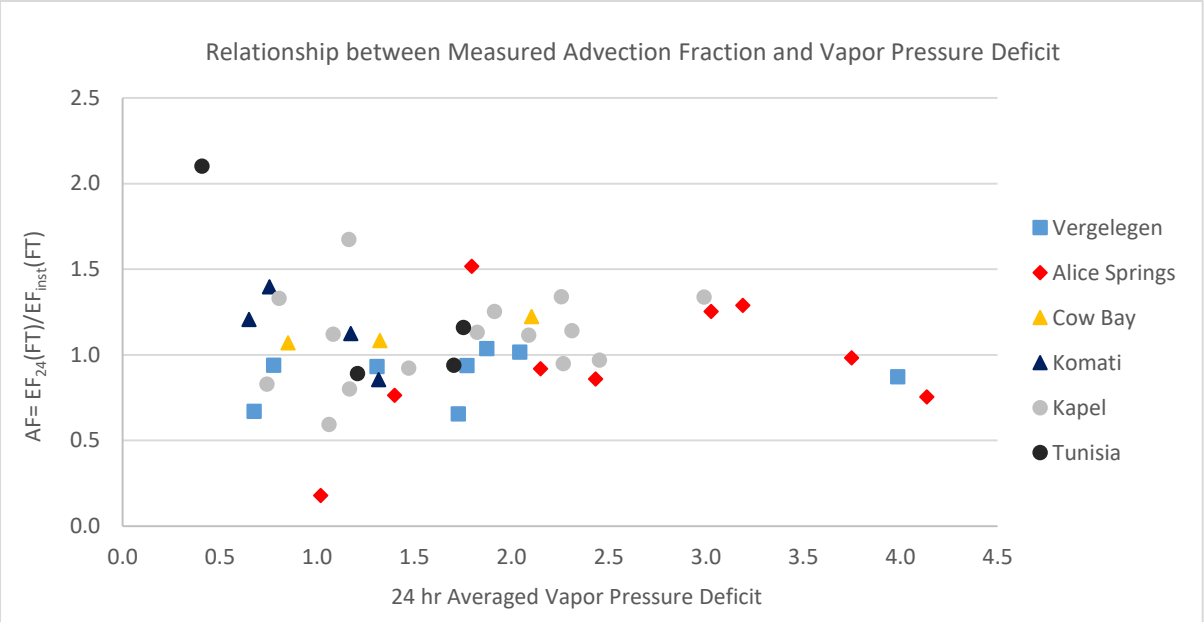

Figure 30: Relationship between advection factors, calculated from flux tower measurements as EF_{inst}/EF_{24}, and 24 hr averaged vapor pressure deficits.

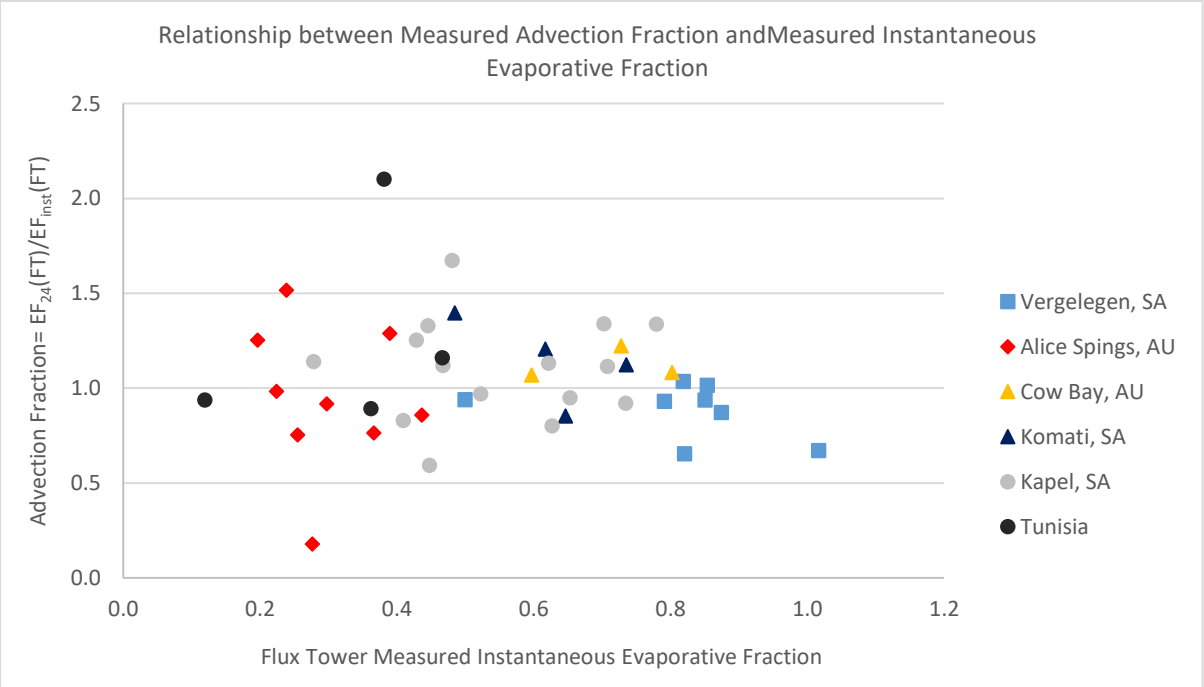

Figure 31: Relationship between advection factors, calculated from flux tower measurements as EF_{inst}/EF_{24}, and instantaneous evaporative fractions.